TECHNISCHE UNIVERSITÄT WIEN

DIPLOMARBEIT

Stable finite element methods for the Reynolds equation in elastohydrodynamic lubrication problems

ausgeführt zum Zwecke der Erlangung des akademischen Grades
eines Master of Science unter der Leitung von

Prof. Dr. Joachim Schöberl
E101 – Institut für Analysis und Scientific Computing

eingereicht an der Technischen Universität Wien
Fakultät für Mathematik und Geoinformation
von

Christoph Leonhartsberger
[redacted]

October 24, 2025

Eidesstaatliche Erklärung

Ich erkläre an Eides statt, dass ich die vorliegende Diplomarbeit selbstständig und ohne fremde Hilfe verfasst, andere als die angegebenen Quellen und Hilfsmittel nicht benutzt bzw. die wörtlich oder sinngemäß entnommenen Stellen als solche kenntlich gemacht habe.

Wien, am 21.10.2025

Unterschrift	Unterschrift des Betreuers

Abstract

This thesis focuses on the development of stable finite element methods for the Reynolds equation in elastohydrodynamic lubrication (EHL) problems. Building upon existing stabilized methods for convection-diffusion problems, a hybrid discontinuous Galerkin (HDG) and a hybrid mixed three-field (HM3F) formulation are introduced and compared with the streamline upwind Petrov-Galerkin (SUPG) method. Furthermore, a mass-conserving cavitation model based on the Jakobsson-Floberg-Olsson (JFO) conditions is presented. The coupling of the Reynolds equation with elasticity, film thickness and load balance equations to obtain the EHL system is discussed for circular contact problems and problems with arbitrary geometries. The computational performance and the stability of the different finite element methods is assessed through numerical experiments.

Acknowledgements

First, I want to express my gratitude to my supervisor Prof. Dr. Joachim Schöberl for his support and guidance throughout the past years. He sparked my interest in numerical methods and gave me the opportunity to work on several exciting projects during my studies as a part-time employee at CERBSim GmbH.

I would also like to thank Christopher Lackner for organizing the internship with AC2T research GmbH for this thesis and for the fruitful discussions we had during that time.

Special thanks to Christoph Wintersteiger from AC2T research GmbH for his support and time during my internship and proofreading this thesis.

Further, I want to thank my colleagues Rafael and Sebastian for enjoyable studying sessions and the great time we had together at the university.

Most importantly I want to thank my family for their continuous support and belief in me.

A significant part of this work was carried out as part of the COMET Centre InTribology (FFG no. 906860), a project of the "Excellence Centre for Tribology" (AC2T research GmbH). InTribology is funded within the COMET – Competence Centres for Excellent Technologies Programme by the federal ministries BMIMI and BMWET as well as the federal states of Niederösterreich and Vorarlberg based on financial support from the project partners involved. COMET is managed by The Austrian Research Promotion Agency (FFG).

This research was co-funded by the European Union under the Horizon Europe programme within SiToLub project (Simulation Tools for the design of safe and sustainable Lubricants) with Grant Agreement No. 101138807.

Co-funded by the European Union

Views and opinions expressed are however those of the author(s) only and do not necessarily reflect those of the European Union or European Research Executive Agency. Neither the European Union nor the granting authority can be held responsible for them.

Contents

Chapter 1

Introduction

Elastohydrodynamic lubrication (EHL) simulations are essential in the design and optimization of machine elements such as gears or bearings. Predicting the pressure distribution and film thickness in the contact area of two bodies in relative motion allows to assess the performance and durability of these components. The mathematical model for EHL problems consists of a coupled system of partial differential equations: the Reynolds equation, which describes the pressure distribution in the lubricant film, the film thickness equation, which accounts for the elastic deformation of the contacting bodies and the load balance equation, which ensures that the generated pressure balances the external load. The nonlinearity of the Reynolds equation due to pressure-dependent viscosity and density of the lubricant, as well as the coupling with the elasticity problem in the film thickness equation, pose significant challenges for numerical simulations. High loaded contacts lead to convection dominance in the Reynolds equation, which requires stabilization techniques to avoid oscillations in the pressure solution. The main goal of this thesis is to develop and analyze stable finite element methods for solving the Reynolds equation in EHL problems. In [1] the proposed residual-based stabilized formulations are the streamline upwind Petrov-Galerkin and the Galerkin least squares formulations. Well-known stabilized formulations for convection-diffusion problems such as hybridized discontinuous Galerkin formulations [2] and hybridized mixed discontinuous Galerkin formulations [3] are the basis for the methods proposed in this thesis. In particular, we will build upon the ideas presented in these works to develop new stabilized methods for the Reynolds equation in EHL problems and compare their performance with existing methods. Another point of interest of this thesis is a mass-conserving cavitation model based on the Jakobsson-Floberg-Olsson (JFO) conditions [4, 5], which yields more accurate results in the cavitated region compared to the commonly used Reynolds boundary conditions.

Outline of the thesis

In chapter 2 we introduce the governing equations of elastohydrodynamic lubrication problems. Starting from the compressible Navier-Stokes equations, we derive the Reynolds equation and present various models for viscosity and density of the lubricant. To complete the description of the Reynolds problem, we discuss boundary conditions for the pressure and present two cavitation models. We close the EHL system by incorporating the film thickness and the load balance equation.

In chapter 3 we present different finite element methods for the Reynolds equation. Starting from a standard Galerkin (CG) formulation we introduce stabilized methods such as the streamline upwind Petrov-Galerkin (SUPG) method, a hybrid discontinuous Galerkin (HDG) formulation and a hybrid mixed three-field method (HM3F).

Numerical results for benchmark problems are presented in chapter 4. We compare the performance of the different finite element methods introduced in chapter 3 in terms of accuracy and computational efficiency.

Chapter 2

Equations describing elastohydrodynamic lubrication problems

This chapter introduces the mathematical model for elastohydrodynamic lubrication (EHL) problems. We start with the derivation of the Reynolds equation from the compressible Navier-Stokes equations and state different models describing viscosity and density of the lubricant. To complete the description of the Reynolds problem on the contact domain we specify the boundary conditions for the pressure and discuss two cavitation models in section 2.1.2. The film thickness equation is presented in section 2.2 where an elasticity problem has to be considered. This equation describes the gap between the surfaces of the two bodies in contact. The load balance equation is introduced in section 2.3 as an integral constraint for the pressure distribution. It ensures that the generated pressure in the lubricant film is sufficient to balance the external load.

2.1 Reynolds equation

The Reynolds equation describes the pressure distribution in the lubricant film. Similar to [6] and [1] we derive the Reynolds equation from the compressible Navier-Stokes equations under the assumptions that

1. the body forces are negligible,
2. the flow is laminar,
3. the lubricant is Newtonian,
4. inertia and surface tension forces are negligible,

5. the lubricant's viscosity and density are constant across the film thickness,
6. no slip conditions are applied at the boundary surfaces,
7. the film thickness is small compared to the other dimensions of the domain.

We denote the velocity field of the lubricant as $\mathbf{u} := (u, v, w)$, the pressure as p, the density as $\rho := \rho(p)$ and the viscosity as $\mu := \mu(p)$. The compressible Navier-Stokes equations in strong form read as

$$\begin{cases} \frac{\partial \rho}{\partial t} + \operatorname{div}(\rho \mathbf{u}) &= 0, & \text{(mass)} \\ \rho\left(\frac{\partial \mathbf{u}}{\partial t} + (\mathbf{u}\cdot\nabla)\mathbf{u}\right) &= -\nabla p + \operatorname{div}(\boldsymbol{\tau}) + \rho\mathbf{f}, & \text{(momentum)} \end{cases} \tag{2.1}$$

where $\boldsymbol{\tau}$ is the stress tensor and $\mathbf{f}$ are the body forces. The stress tensor for a Newtonian fluid is given by

$$\boldsymbol{\tau} = \mu\left(\nabla\mathbf{u} + \nabla\mathbf{u}^T\right) - \frac{2}{3}\mu\left(\operatorname{div}(\mathbf{u})\right)\mathbf{I}, \tag{2.2}$$

with the identity matrix $\mathbf{I}$. Using the assumptions 1. and 4. from above and considering a steady state situation we can simplify the Navier-Stokes equations (2.1) to

$$\begin{cases} \operatorname{div}(\rho\mathbf{u}) &= 0, \\ -\nabla p + \operatorname{div}(\boldsymbol{\tau}) &= 0. \end{cases} \tag{2.3}$$

Inserting the terms of the stress tensor (2.2) into the momentum equation of (2.3) yields

$$\begin{cases} \frac{\partial p}{\partial x} &= -\frac{2}{3}\frac{\partial}{\partial x}\left(\mu\left(\frac{\partial u}{\partial x} + \frac{\partial v}{\partial y} + \frac{\partial w}{\partial z}\right)\right) + 2\frac{\partial}{\partial x}\left(\mu\frac{\partial u}{\partial x}\right) \\ &\quad + \frac{\partial}{\partial y}\left(\mu\left(\frac{\partial u}{\partial y} + \frac{\partial v}{\partial x}\right)\right) + \frac{\partial}{\partial z}\left(\mu\left(\frac{\partial u}{\partial z} + \frac{\partial w}{\partial x}\right)\right), \\ \frac{\partial p}{\partial y} &= -\frac{2}{3}\frac{\partial}{\partial y}\left(\mu\left(\frac{\partial u}{\partial x} + \frac{\partial v}{\partial y} + \frac{\partial w}{\partial z}\right)\right) + 2\frac{\partial}{\partial y}\left(\mu\frac{\partial v}{\partial y}\right) \\ &\quad + \frac{\partial}{\partial x}\left(\mu\left(\frac{\partial u}{\partial y} + \frac{\partial v}{\partial x}\right)\right) + \frac{\partial}{\partial z}\left(\mu\left(\frac{\partial v}{\partial z} + \frac{\partial w}{\partial y}\right)\right), \\ \frac{\partial p}{\partial z} &= -\frac{2}{3}\frac{\partial}{\partial z}\left(\mu\left(\frac{\partial u}{\partial x} + \frac{\partial v}{\partial y} + \frac{\partial w}{\partial z}\right)\right) + 2\frac{\partial}{\partial z}\left(\mu\frac{\partial w}{\partial z}\right) \\ &\quad + \frac{\partial}{\partial x}\left(\mu\left(\frac{\partial u}{\partial z} + \frac{\partial w}{\partial x}\right)\right) + \frac{\partial}{\partial y}\left(\mu\left(\frac{\partial v}{\partial z} + \frac{\partial w}{\partial y}\right)\right). \end{cases} \tag{2.4}$$

Introducing a parameter $\epsilon = h_0/L$, where h_0 is the characteristic film thickness and L is the characteristic length of the contact area, equation (2.4) can be nondimensionalized. By analyzing the asymptotic behavior with respect to ϵ, higher

order terms can be neglected. For the full derivation we refer to [6] where this is done in detail for the iso-viscuous and incompressible case. Given that the film thickness is small compared to the other dimensions of the domain, we rescale the velocities u and v with $\frac{1}{u_0}$ and w with $\frac{1}{\epsilon u_0}$, where u_0 is a characteristic velocity. This results in a scaling of the derivatives in x and y direction with $\frac{1}{L}$ compared to the derivative in z direction with $\frac{1}{\epsilon L}$. Thus the derivatives in z direction are dominant and the terms in (2.4) can be simplified to

$$\begin{cases} \frac{\partial p}{\partial x} &= \frac{\partial}{\partial z}\left(\mu\left(\frac{\partial u}{\partial z}\right)\right), \\ \frac{\partial p}{\partial y} &= \frac{\partial}{\partial z}\left(\mu\left(\frac{\partial v}{\partial z}\right)\right), \\ \frac{\partial p}{\partial z} &= 0, \end{cases} \tag{2.5}$$

where we rescaled p with $\frac{1}{\epsilon^s}$ using $s = 2$. Choosing $s > 2$ would result in a pure Poiseuille flow without a pressure gradient, while choosing $s < 2$ would lead to a plain Couette flow. Since there holds

$$\frac{\partial p}{\partial z} = 0,$$

the terms on the right hand side of the first two equations in (2.5) result in

$$\frac{\partial}{\partial z}\left(\mu\left(\frac{\partial u}{\partial z}\right)\right) = \frac{\partial}{\partial z}(\mu)\frac{\partial u}{\partial z} + \mu\frac{\partial^2 u}{\partial z^2} = \frac{\partial \mu}{\partial p}\frac{\partial p}{\partial z} + \mu\frac{\partial^2 u}{\partial z^2} = \mu\frac{\partial^2 u}{\partial z^2}$$

and we can integrate those equations twice with respect to z to obtain

$$\begin{aligned} u(x,y,z) &= \frac{1}{2\mu}\frac{\partial p}{\partial x}z^2 + A_{11}(x,y)z + A_{12}(x,y), \\ v(x,y,z) &= \frac{1}{2\mu}\frac{\partial p}{\partial y}z^2 + A_{21}(x,y)z + A_{22}(x,y), \end{aligned} \tag{2.6}$$

where $A_{ij}(x,y)$ are functions that have to be determined via the boundary conditions of u and v. The no-slip condition states that

$$\begin{aligned} \mathbf{U}_l &= \begin{bmatrix} u\left(x,y,h_l(x,y)\right) \\ v\left(x,y,h_l(x,y)\right) \end{bmatrix} = \begin{bmatrix} u_l(x,y) \\ v_l(x,y) \end{bmatrix}, \\ \mathbf{U}_u &= \begin{bmatrix} u\left(x,y,h_u(x,y)\right) \\ v\left(x,y,h_u(x,y)\right) \end{bmatrix} = \begin{bmatrix} u_u(x,y) \\ v_u(x,y) \end{bmatrix}, \end{aligned}$$

where h_l and h_u are the lower and upper surface profiles respectively and u_l and u_u denote the corresponding surface velocities. Solving this linear system for $A_{ij}(x,y)$

and inserting the results into (2.6) leads to

$$\mathbf{u} = \begin{bmatrix} u(x,y,z) \\ v(x,y,z) \end{bmatrix} = \begin{bmatrix} \frac{(z-h_l)(z-h_u)}{2\mu}\frac{\partial p}{\partial x} + (u_u - u_l)\frac{z-h_l}{h_u-h_l} + u_l \\ \frac{(z-h_l)(z-h_u)}{2\mu}\frac{\partial p}{\partial y} + (v_u - v_l)\frac{z-h_l}{h_u-h_l} + v_l \end{bmatrix}. \tag{2.7}$$

If we consider the lower body to be planar and aligned with the xy-plane, i.e. $h_l(x,y) = 0$, the above equation simplifies to

$$\mathbf{u} = \begin{bmatrix} u(x,y,z) \\ v(x,y,z) \end{bmatrix} = \begin{bmatrix} \frac{z(z-h_u)}{2\mu}\frac{\partial p}{\partial x} + (u_u - u_l)\frac{z}{h_u} + u_l \\ \frac{z(z-h_u)}{2\mu}\frac{\partial p}{\partial y} + (v_u - v_l)\frac{z}{h_u} + v_l \end{bmatrix},$$

which is the same expression as in [1]. To obtain the Reynolds equation we recall the conservation of mass equation from (2.3) and integrate over the film thickness which leads to

$$\int_{h_l}^{h_u} \frac{\partial(\rho u)}{\partial x}\,dz + \int_{h_l}^{h_u} \frac{\partial(\rho v)}{\partial y}\,dz + \int_{h_l}^{h_u} \frac{\partial(\rho w)}{\partial z}\,dz = 0. \tag{2.8}$$

The last term in (2.8) can be simplified by using the fundamental theorem of calculus which then reads as

$$\int_{h_l}^{h_u} \frac{\partial(\rho w)}{\partial z}\,dz = \rho w_u - \rho w_l,$$

where $w_u = w(x,y,h_u(x,y))$ and $w_l = w(x,y,h_l(x,y))$. The kinematic boundary condition for the vertical velocity at the upper and lower surface is given by

$$\begin{aligned} w_u &= u_u\frac{\partial h_u}{\partial x} + v_u\frac{\partial h_u}{\partial y}, \\ w_l &= u_l\frac{\partial h_l}{\partial x} + v_l\frac{\partial h_l}{\partial y}. \end{aligned} \tag{2.9}$$

Using the Leibniz rule, which states that

$$\frac{\partial}{\partial x}\left(\int_{a(x)}^{b(x)} f(x,z)\,dz\right) = \int_{a(x)}^{b(x)} \frac{\partial f}{\partial x}(x,z)\,dz + f(x,b(x))\frac{db}{dx} - f(x,a(x))\frac{da}{dx},$$

and the equations (2.9) for w_u and w_l, we can rewrite (2.8) as

$$\frac{\partial}{\partial x}\left(\int_{h_l}^{h_u} \rho u\,dz\right) + \frac{\partial}{\partial y}\left(\int_{h_l}^{h_u} \rho v\,dz\right) = 0, \tag{2.10}$$

where the boundary terms vanish as they coincide with the terms from the kinematic boundary condition. Next, we perform one of the integrals over the film thickness in (2.10) using the velocity profile (2.7). We only show the calculations for the u-component, which reads as

$$
\begin{aligned}
\int_{h_l}^{h_u} \rho u \, dz &= \int_{h_l}^{h_u} \rho \left(\frac{(z-h_l)\,(z-h_u)}{2\mu} \frac{\partial p}{\partial x} + (u_u - u_l) \frac{z-h_l}{h_u - h_l} + u_l \right) dz \\
&= \frac{\rho}{2\mu} \frac{\partial p}{\partial x} \int_{h_l}^{h_u} z^2 - z h_l - z h_u + h_u h_l \, dz \\
&\quad + \frac{\rho(u_u - u_l)}{h_u - h_l} \int_{h_l}^{h_u} z - h_l \, dz + \rho u_l [z]_{h_l}^{h_u} \, dz \\
&= \frac{\rho}{2\mu} \frac{\partial p}{\partial x} \left[\frac{z^3}{3} - \frac{h_l z^2}{2} - \frac{h_u z^2}{2} + h_u h_l z \right]_{h_l}^{h_u} \\
&\quad + \frac{\rho(u_u - u_l)}{h_u - h_l} \left[\frac{z^2}{2} - h_l z \right]_{h_l}^{h_u} + \rho u_l [z]_{h_l}^{h_u} \\
&= \frac{\rho}{2\mu} \frac{\partial p}{\partial x} \left(\frac{h_u^3 - h_l^3}{3} - \frac{h_l (h_u^2 - h_l^2)}{2} - \frac{h_u (h_u^2 - h_l^2)}{2} + h_u h_l (h_u - h_l) \right) \\
&\quad + \frac{\rho(u_u - u_l)}{h_u - h_l} \left(\frac{h_u^2 - h_l^2}{2} - h_l (h_u - h_l) \right) + \rho u_l (h_u - h_l) \\
&= \frac{\rho}{2\mu} \frac{\partial p}{\partial x} \left(\frac{(h_l - h_u)^3}{6} \right) + \frac{\rho(u_u - u_l)}{h_u - h_l} \left(\frac{(h_u - h_l)^2}{2} \right) + \rho u_l (h_u - h_l) \\
&= \frac{\rho (h_l - h_u)^3}{12\mu} \frac{\partial p}{\partial x} + \frac{\rho (u_u - u_l)(h_u - h_l)}{2} + \rho u_l (h_u - h_l) \\
&= -\frac{\rho h^3}{12\mu} \frac{\partial p}{\partial x} + \frac{\rho h}{2} (u_u - u_l) + \rho u_l h \\
&= -\frac{\rho h^3}{12\mu} \frac{\partial p}{\partial x} + \frac{\rho h}{2} (u_u + u_l),
\end{aligned}
$$

where we defined $h := h_u - h_l$ as the film thickness and used assumption 5, which states that the density and the viscosity are constant across the film thickness. Inserting the velocity profile (2.7) for both components into (2.8) therefore yields

$$
\begin{aligned}
&- \frac{\partial}{\partial x} \left(\frac{\rho h^3}{12\mu} \frac{\partial p}{\partial x} \right) - \frac{\partial}{\partial y} \left(\frac{\rho h^3}{12\mu} \frac{\partial p}{\partial y} \right) \\
&+ \frac{\partial}{\partial x} \left(\frac{\rho h}{2} (u_u + u_l) \right) + \frac{\partial}{\partial y} \left(\frac{\rho h}{2} (v_u + v_l) \right) = 0.
\end{aligned} \tag{2.11}
$$

Defining the mean velocities

$$u_m := \frac{u_u + u_l}{2} \quad \text{and} \quad v_m := \frac{v_u + v_l}{2}$$

we obtain the Reynolds equation

$$-\frac{\partial}{\partial x}\left(\frac{\rho h^3}{\mu}\frac{\partial p}{\partial x}\right) - \frac{\partial}{\partial y}\left(\frac{\rho h^3}{\mu}\frac{\partial p}{\partial y}\right) + \frac{\partial}{\partial x}\left(12\rho h u_m\right) + \frac{\partial}{\partial y}\left(12\rho h v_m\right) = 0.$$

A more compact form of the Reynolds equation reads as

$$-\operatorname{div}\left(\frac{h^3\rho(p)}{\mu(p)}\nabla p - 12hU\rho(p)\right) = 0, \tag{2.12}$$

where $U = (u_m, v_m)^T$ denotes the mean velocity field. Here we write $\rho(p)$ and $\mu(p)$ to emphasize the pressure dependency of the density and viscosity. By defining

$$\begin{aligned} \varepsilon(p) &:= \frac{h^3\rho(p)}{\mu(p)}, \\ \beta &:= 12hU, \end{aligned} \tag{2.13}$$

we can rewrite (2.12) as

$$-\operatorname{div}\left(\varepsilon(p)\nabla p - \beta\rho(p)\right) = 0, \tag{2.14}$$

which is the form we will utilize in the numerical discretization chapter.

2.1.1 Viscosity and density models

The lubricant properties used in the Reynolds equation can be modelled with different pressure and temperature dependent approaches. In this work we consider the same models as mentioned in [1] for viscosity and density since they are widely used in EHL simulations and it allows the comparison of the results. The density functions are less critical as they only lead to slight variations for high pressure. The viscosity models on the other hand yield significant differences with increasing pressure making some of them not suitable for high loaded contacts. The following cited models are written in a pressure and temperature dependent form, but we will mostly consider isothermal conditions, i.e. $T = T_0$.

Dowson-Higginson model

The model from [7] is the most used density variation relationship in EHL. It is given by

$$\rho(p,T) = \rho_R\left[1 + \frac{0.6\cdot 10^{-9}p}{1 + 1.7\cdot 10^{-9}p} - \beta_{DH}\left(T - T_R\right)\right]. \tag{2.15}$$

Here $\rho(p,T)$ denotes the lubricants density at a given pressure p and temperature T, $\rho_R = \rho\,(p = p_R = 0, T = T_R)$ is the zero-pressure density at the reference temperature T_R and β_{DH} is the density-temperature coefficient. This strictly empirical model is used due to its simplicity.

Barus model

The Barus model [8] is a simple exponential model for the viscosity-pressure relationship. It is the isothermal version of the Cheng model [9] and has the form

$$\mu(p) = \mu_R \exp(\alpha p),$$

where $\mu_R = \mu\,(p = p_R = 0)$ is the zero-pressure viscosity and α is the pressure-viscosity coefficient. This model is only suitable for low pressure ranges as it overestimates the viscosity for high pressures.

Roelands model

A more accurate model was proposed by Roelands [10], which reads as

$$\mu(p,T) = \mu_R \exp\Bigg\{ (\ln(\mu_R) + 9.67)\cdot \Big[-1 + (1 + 5.1\cdot 10^{-9} p)^{Z_0} \Big(\frac{T-138}{T_R-138}\Big)^{-S_0} \Big] \Bigg\}, \tag{2.16}$$

$$\text{where} \quad Z_0 = \frac{\alpha}{[5.1\cdot 10^{-9}\,(\ln(\mu_R) + 9.67)]}, \qquad S_0 = \frac{\beta_{\text{Roe}}\,(T_R - 138)}{\ln(\mu_R) + 9.67}.$$

According to [1] this model is valid for moderately high pressures but similar to the Barus model it overestimates the viscosity for high loaded contacts. Both of the mentioned viscosity models are strictly empirical.

Modified WLF model

A more physical model based on the work of Williams, Landel and Ferry [11] and Yasutomi, Bair and Winer [12] is the modified WLF model. This model is valid for a wide range of pressures and temperatures and is given by

$$\mu(p,T) = \mu_g \cdot 10^{\frac{-C_1\cdot(T-T_g(p))\cdot F(p)}{C_2+(T-T_g(p))\cdot F(p)}}, \tag{2.17}$$

$$\text{where} \quad T_g(p) = T_g(0) + A_1 \ln(1 + A_2 p),$$
$$F(p) = 1 - B_1 \ln(1 + B_2 p),$$

A_1, A_2, B_1, B_2, C_1 and C_2 are constants characterizing the fluid and μ_g is the viscosity at the glass transition temperature T_g. The function $T_g(p)$ denotes the variation of the glass transition temperature based on experimental data whereas $F(p)$ represents the variation of the thermal expansion coefficient with pressure. This model is more complex than the previous ones but provides a more accurate representation of the viscosity for high loaded contacts. Due to the difficult characterization of the constants of the fluid it is not as widely used as the Barus or Roelands model.

2.1.2 Boundary conditions and cavitation models

As the Reynolds equation is a partial differential equation we need to define boundary conditions for the pressure at the boundary of the contact domain Ω_c. A common choice is to set the pressure to zero at the boundary

$$p = 0 \text{ on } \partial\Omega_c.$$

This means we assume the pressure to be equal to the ambient pressure at the boundary. Furthermore we consider the lubricant to be at liquid state, which states that pressures below the vapour pressure are physically impossible. This yields cavitation and constant pressure in the cavitated region equal to the vapour pressure. The cavitation boundary condition (Reynolds' boundary condition) then reads as

$$p \geq 0 \text{ in } \Omega_c, \quad p = \nabla \cdot \vec{n_c} \text{ on the cavitation boundary,}$$

where $\vec{n_c}$ is the outward normal vector of the outlet boundary of the contact domain Ω_c (cavitation boundary). This leads to a free boundary problem as the location of the cavitation boundary is not known in advance. To handle this problem we introduce two different approaches. The first one is a penalty method as described in [1] and the second one is a mass-conserving approach similar to the one presented in [13, 14].

Penalty method

To satisfy the cavitation boundary condition a penalty term is added to the Reynolds equation since we require pressure positivity. Therefore, we introduce $p^- = \min(p, 0)$ and ξ as a sufficiently large positive parameter. The additional penalty term reads as ξp^- and is only active for negative pressures. This penalty

term tries to enforce pressure positivity by adding mass to the system (not physically correct). The parameter ξ has to be chosen large enough to restrict the pressure to be positive, which can usually not be achieved but it results in small negative pressures. Although choosing ξ too small leads to higher negative pressure values, large values for ξ result in slower convergence.

Mass-conserving method

Another approach is a mass-conserving method which is obtained by altering the viscosity and density functions. The idea is to damp density and viscosity for negative pressures with a function f. This method satisfies the JFO condition (Jakobsson-Floberg-Olsson condition), which is essentially the Reynolds boundary condition with mass-conservation in the cavitated region. For a more detailed discussion we refer to [4, 5]. The damping function used in [13] is given by

$$f(p) = \begin{cases} 1, & p > 0, \\ 3\left(\frac{p}{\eta}\right)^2 - 2\left(\frac{p}{\eta}\right)^3, & \eta < p \leq 0, \\ 0, & p \leq \eta, \end{cases}$$

where η is a factor for the transition zone of the scaling parameter between non-cavitated density/viscosity and the minimum density/viscosity. To avoid numerical issues with zero values the parameter α is introduced and density and viscosity are modified such that

$$\rho(p) = (f(p) + \alpha) \cdot \frac{\rho_0(p)}{1+\alpha},$$
$$\eta(p) = (f(p) + \alpha) \cdot \frac{\eta_0(p)}{1+\alpha},$$

where ρ_0 and μ_0 are the original density and viscosity functions. Instead of using the polynomial function from [13], we define an exponential function to damp density and viscosity leading to the expression

$$f(p) = \begin{cases} 1, & p > 0, \\ \exp(\frac{p}{\eta}), & p \leq 0. \end{cases} \tag{2.18}$$

Here η is a positive parameter which is chosen large initally and after solving the EHL equations it is decreased until a certain negative pressure level is reached. Density and viscosity are then modified as

$$\rho(p) = \rho_0(p) f(p),$$
$$\mu(p) = \mu_0(p) f(p).$$

Note that here we do not need the parameter α as the exponential function is strictly positive.

2.2 Elasticity and film thickness equation

Based on the work of [1] we first consider the film thickness equation of a circular contact by reducing the two-body problem to a one-body problem and using analytic expressions for the distance calculation of the undeformed surfaces. Then we introduce a more general approach for arbitrary geometries by considering both bodies, calculating this distance numerically and solving the elasticity problem for each body. The film thickness mainly depends on three parameters. The first one is the rigid body displacement h_0, which describes the minimal distance between the two undeformed surfaces. The second one is the geometry of the contact surfaces, where the distance of the surfaces is usually approximated with a parabolic profile, and the third one is the elastic displacement of the surfaces due to the applied pressure. For circular contacts the film thickness can be expressed as

$$h(x,y) = h_0 + \frac{x^2+y^2}{2R} + \delta(x,y), \tag{2.19}$$

where $\delta(x,y)$ is the elastic deflection term and R is the radius of curvature of the contact surface. The term

$$\frac{x^2+y^2}{2R}$$

describes an approximation to the distance between the two undeformed surfaces assuming a parabolic profile. An advantage of this approach is that only one body needs to be considered and the distance is calculated analytically. In this case the elasticity calculation to obtain $\delta(x,y)$ is performed on a planar body with equivalent material parameters. The material properties, i.e. Young's modulus and Poisson's ratio, change to

$$\begin{aligned} E &= \frac{{E_1}^2 E_2 (1+\nu_2)^2 + {E_2}^2 E_1 (1+\nu_1)^2}{\left[E_1(1+\nu_2) + E_2(1+\nu_1)\right]^2}, \\ \nu &= \frac{E_1\nu_2(1+\nu_2) + E_2\nu_1(1+\nu_1)}{E_1(1+\nu_2) + E_2(1+\nu_1)}, \end{aligned} \tag{2.20}$$

where E_1, E_2 are the Young's moduli and ν_1, ν_2 are the Poisson's ratios of the two bodies, respectively. If we consider two bodies with the same material properties $E_1 = E_2$ and $\nu_1 = \nu_2$, the equivalent values are given by

$$E = \frac{E_1}{2}, \quad \nu = \nu_1.$$

These parameters are then used in the elasticity problem to calculate the elastic deformation $\delta(x,y)$. Since this work focuses on the development of stable finite

element methods for the Reynolds equation we will not go into details regarding the elasticity problem and refer to [15] for the linear elasticity equations. The elasticity problem for the EHL simulation in strong form reads as

$$\begin{cases} \nabla \cdot \sigma = 0 & \text{in } \Omega, \\ \sigma = \mathbb{C}\,\epsilon_s(u) & \text{in } \Omega, \\ u = 0 & \text{on } \Omega_b, \\ \sigma_n = -p & \text{on } \Omega_c, \\ \sigma_n = 0 & \text{on } \partial\Omega \setminus (\Omega_b \cup \Omega_c), \end{cases} \tag{2.21}$$

where σ denotes the stress tensor, $\epsilon_s(u)$ the linearized strain tensor and $\mathbb{C}$ the compliance matrix, which is a stress-strain relation dependent on material laws. Ω_c is the contact boundary and Ω_b is the part of the domain where Dirichlet boundary conditions are applied. Figure 2.1 illustrates a ball on plate contact problem, where the ball is represented by a half circle and the plate is a rectangle. Ω (gray), Ω_c (red) and Ω_b (blue) are marked for a two-body and the equivalent single-body setup.

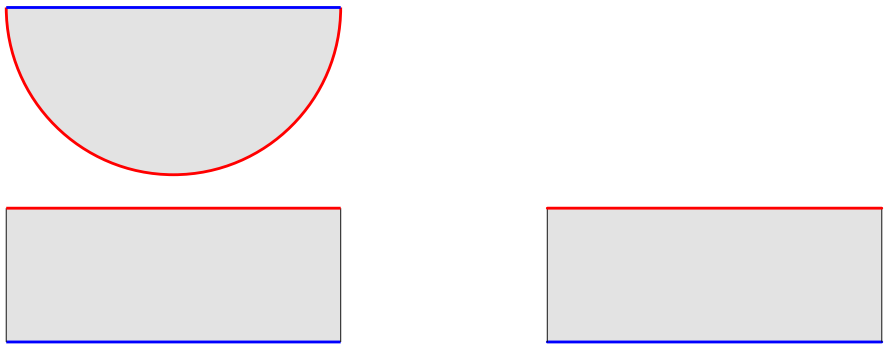

(a) Two-body setup for a ball on plate problem

(b) Single-body setup for a ball on plate problem

Figure 2.1: Ball on plate problem: Boundaries for two-body and single-body setup

Solving this problem yields the displacement u of the body, which is then used to calculate the elastic displacement $\delta(x, y)$ in the film thickness equation (2.19). The elastic displacement

$$\delta(x, y) = -u(x, y) \cdot n_{\text{surf}} \tag{2.22}$$

is given by the deformation in direction of the outward pointing surface normal n_{surf} of the contact domain.

As mentioned before we can also consider both bodies for the film thickness equation and the elasticity problem. In this case the distance of the undeformed

surfaces $\widetilde{h}$ is calculated numerically. The film thickness equation (2.19) then reads as

$$h(x,y) = h_0 + \widetilde{h}(x,y) + \delta_1(x,y) + \delta_2(x,y), \tag{2.23}$$

where $\delta_1(x,y)$ and $\delta_2(x,y)$ are the elastic deformations of the two bodies, respectively. The distance $\widetilde{h}(x,y)$ is calculated by searching for each point (x,y) of the contact domain Ω_c the closest point on the surface of the second body and computing the distance. A possible implementation is described in section 4.2.2. The elasticity problem has to be solved for both bodies, which means we have to solve (2.21) for each body with the corresponding material parameters and boundary conditions, where the pressure p is now applied to both contact surfaces. The elastic deformations $\delta_1(x,y)$ and $\delta_2(x,y)$ are calculated similar to equation (2.22), where we use a different formulation for the surface normal n_{surf} of each body. Denoting for a point p_1 of the contact surface the closest point of the second body as p_2, the surface normal is given by

$$n_{\text{surf}} = \frac{p_2 - p_1}{\|p_2 - p_1\|}.$$

Using this normal vector we obtain the elastic displacements of both bodies as

$$\begin{aligned} \delta_1(x,y) &= -u_1(x,y) \cdot n_{\text{surf}}, \\ \delta_2(x,y) &= u_2(x,y) \cdot n_{\text{surf}}, \end{aligned} \tag{2.24}$$

where $u_1(x,y)$ and $u_2(x,y)$ are the deformations of the first and second body, respectively. Note that the sign of $\delta_2(x,y)$ changes, since the normal vector of this surface points in the opposite direction and we are using the same normal vector as for the other body. Inserting equations (2.24) into the film thickness equation (2.23) yields

$$h(x,y) = h_0 + \widetilde{h}(x,y) + (u_2(x,y) - u_1(x,y)) \cdot n_{\text{surf}}.$$

As an example we once again consider the ball on plate geometry. The initial configuration is shown in Figure 2.2a, where h_0 is the rigid body displacement and $\widetilde{h}(p_1)$ is the distance of the two undeformed surfaces at point p_1. In Figure 2.2b the deformed configuration due to the applied pressure to the surfaces is shown and the terms $\delta_1(x,y)$ and $\delta_2(x,y)$ are illustrated.

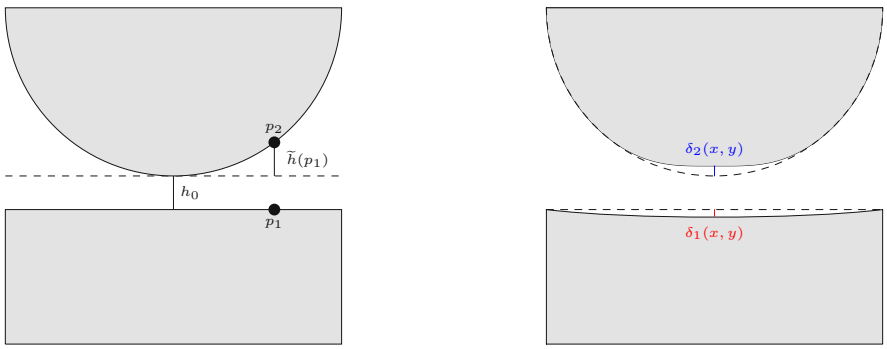

(a) Initial configuration of a ball on plate geometry

(b) Ball on plate geometry after deformation

Figure 2.2: Ball on plate geometry with film thickness equation terms.

2.3 Load balance equation

The load balance equation is an integral constraint for the pressure distribution in the contact domain Ω_c. It ensures that the total applied force F is equal to the generated pressure in the contact domain, which can be expressed as

$$\int_{\Omega_c} p \, d\Omega = F. \tag{2.25}$$

This equation determines the parameter h_0 of the film thickness equation (2.19).

2.4 Moes parameter

In this section we define dimensionless parameters to characterize a circular contact EHL problem. Similar to [1] we use the parameters introduced by [16] and [17], which uniquely determine the problem. We start by defining the reduced elastic modulus

$$E' = \frac{2}{\frac{1-\nu_1^2}{E_1} + \frac{1-\nu_2^2}{E_2}}, \tag{2.26}$$

where E_1, E_2 are the Young's moduli and ν_1, ν_2 are the Poisson's ratios of the two bodies. The parameters by Hamrock and Dowson are then given by

$$W_{HD} = \frac{F}{E'R^2}, \quad G_{HD} = \alpha E', \quad \text{and} \quad U_{HD} = \frac{\mu_0 u_m}{E'R},$$

where F is the applied load, R is the equivalent radius of curvature and α is the pressure-viscosity coefficient. Using these expressions the Moes parameters read as

$$M = W_{HD}(U_{HD})^{-\frac{3}{4}} \quad \text{and} \quad L = G_{HD}(2U_{HD})^{\frac{1}{4}}. \tag{2.27}$$

Chapter 3

Finite element formulations

This chapter introduces finite element formulations for the EHL equations focussing on stabilized methods for the Reynolds equation. Starting from a standard Galerkin (CG) formulation, methods like streamline upwind Petrov-Galerkin (SUPG), a hybrid discontinuous Galerkin (HDG) formulation and a hybrid mixed three-field method (HM3F) are presented in the following sections. The section dedicated to the hybrid mixed two-field method (HM2F) only serves as a basis for the HM3F method and is not used in the numerical tests, as it is prone to numerical instabilities for high loaded contacts.

3.1 Basics

Given a domain $\Omega \subseteq \mathbb{R}^d$, $d = 2, 3$ with Lipschitz boundary we start by discretizing the domain with a triangulation $\mathcal{T}_h$. As an example we consider feasible triangulations for a circular and a line contact case:

- Circular contact case: $\Omega \subseteq \mathbb{R}^3$ and $\Omega_c \subseteq \mathbb{R}^2$
  A triangulation can be achieved with tetrahedrons for the $3d$ subdomains and triangles for the $2d$ subdomains which is depicted for a cube in Figure 3.1a and the corresponding contact domain (colored in red) in Figure 3.1b. The top domain represents the contact domain Ω_c, where the Reynolds equation is solved. Figure 3.2 shows a reference element for tetrahedrons and triangles.

- Line contact case: $\Omega \subseteq \mathbb{R}^2$ and $\Omega_c \subseteq \mathbb{R}$
  A triangulation can be achieved with triangles and line elements, respectively. Here we consider a square domain as Ω and the top edge as the contact domain Ω_c.

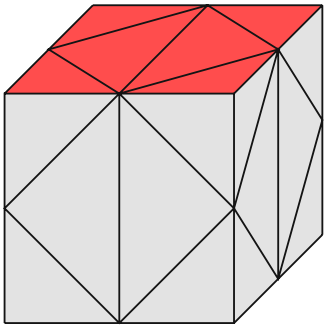

(a) Triangulation of Ω (cube) using tetrahedrons

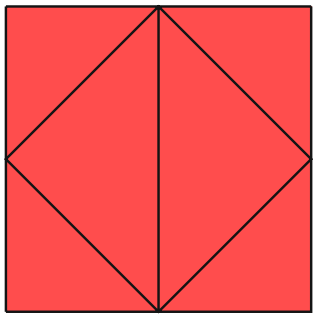

(b) Triangulation of Ω_c (square) using triangles

Figure 3.1: Triangulation for a circular contact case: $\Omega \subseteq \mathbb{R}^3$ and $\Omega_c \subseteq \mathbb{R}^2$

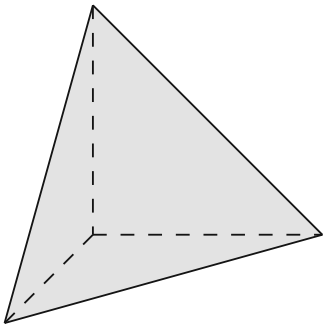

(a) Tetrahedron

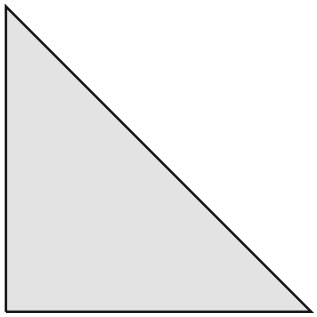

(b) Triangle

Figure 3.2: Reference triangulation elements for a circular contact case: tetrahedron in $\mathbb{R}^3$ and triangle in $\mathbb{R}^2$

For more general discretizations we follow the definitions from [15].

Definition 3.1.1. (Regular triangulation)
We call a triangulation $\mathcal{T}_h$ of Ω regular if

- the elements are non-overlapping $T_i^\circ \cap T_j^\circ = \emptyset$, $T_i \neq T_j \in \mathcal{T}_h$, where T° denotes the interior of T,
- the domain Ω is covered by the elements $\overline{\Omega} = \cup_{T \in \mathcal{T}_h} \overline{T}$,
- the intersection of the elements is either empty, or a common face, edge or vertex of both.

For a given triangulation $\mathcal{T}_h$ we define the interfaces between the elements as $\mathcal{E}_h$ and call $E \in \mathcal{E}_h$ facet.

Definition 3.1.2. (Finite Element)
The triplet $(T, V, \mathcal{N})$ is called a finite element if

- the element domain $T \subset \mathbb{R}^d$ is a bounded and closed set with non-empty interior and piece-wise smooth boundary,
- the space of shape functions V is finite dimensional,
- the set of degrees of freedom (dofs) $\mathcal{N} = \{N_1, \ldots, N_k\}$ is a basis for V^*, the dual space of V.

To define the finite element space we utilize affine mappings $\Phi_T : \hat{T} \to T$ and $\Phi_E : \hat{E} \to E$ as a transformation from the reference element $\hat{T}$ and facet $\hat{E}$ to the physical element T and facet E as in [18]. Now we define the polynomial spaces on the physical element and facet by

$$\mathcal{P}_k(T) := \left\{ v : v = \hat{v} \circ \Phi_T^{-1}, \hat{v} \in \mathcal{P}_k(\hat{T}) \right\},$$
$$\mathcal{P}_k(E) := \left\{ v : v = \hat{v} \circ \Phi_E^{-1}, \hat{v} \in \mathcal{P}_k(\hat{E}) \right\},$$

where $\mathcal{P}_k(\hat{T})$ and $\mathcal{P}_k(\hat{E})$ denote the space of polynomials of order of at most k on the reference element and facet. The set of all piece-wise polynomials on the triangulation $\mathcal{T}_h$ is then given by

$$\mathcal{P}_k(\mathcal{T}_h) := \prod_{T \in \mathcal{T}_h} \mathcal{P}_k(T),$$

and similarly for the facet space $\mathcal{P}_k(\mathcal{E}_h)$. For the weak formulation of the EHL equations we first define the L^2-scalar product and L^2-norm as

$$(u, v)_\Omega := \int_\Omega uv \, d\Omega \quad \text{and} \quad \|u\|_{L^2(\Omega)} := \sqrt{(u, u)_\Omega}. \tag{3.1}$$

This allows us to define $L^2(\Omega)$, $H^1(\Omega)$, $H^s(\Omega)$, and $H(\mathrm{div}, \Omega)$ as

$$L^2(\Omega) := \left\{ v : \Omega \mapsto \mathbb{R} : \|v\|_{L^2(\Omega)} < \infty \right\},$$
$$H^1(\Omega) := \left\{ v \in L^2(\Omega) : \nabla v \in \left[L^2(\Omega)\right]^d \right\},$$
$$H^s(\Omega) := \left\{ v \in L^2(\Omega) : \nabla v \in \left[H^{s-1}(\Omega)\right]^d \right\},$$
$$H(\mathrm{div}, \Omega) := \left\{ v \in \left[L^2(\Omega)\right]^d : \mathrm{div}(v) \in L^2(\Omega) \right\}.$$

We will utilize discontinuous spaces for the weak formulation with higher regularity on each element, which leads to the definition of broken Sobolev spaces.

Definition 3.1.3. (Broken Sobolev space)
Consider a triangulation $\mathcal{T}_h$ of the domain Ω into elements $T \in \mathcal{T}_h$. The space of elementwise $H^s(T)$ functions (broken Sobolev space) is defined as

$$H^s(\mathcal{T}_h) := \left\{ v \in L^2(\Omega), v \in H^s(T) \ \forall T \in \mathcal{T}_h \right\}.$$

3.2 Weak form of the EHL equations

To obtain the weak form of the EHL equations we consider the Reynolds equation (2.14), the elasticity equation (2.21) and the load balance equation (2.25). The Reynolds equation is solved on the contact domain Ω_c, whereas the elasticity equation is solved on the whole domain Ω. The load balance equation is an integral constraint over the contact domain Ω_c. We multiply the strong form of the equations with corresponding test functions and integrate over the respective domains. The linearized elasticity equation in weak form reads as

$$\int_\Omega \mathbb{C}\epsilon_s(u) : \epsilon_s(v)\, d\Omega - \int_{\Omega_c} pn \cdot v\, d\Omega = 0,$$

where v is a test function and n is the outward pointing normal vector of the contact surface. We denote the test functions for the pressure, elastic displacement and rigid body displacement as q, v and w, respectively. After integration by parts of the Reynolds equation and adding the penalty term to ensure pressure positivity the weak form of the EHL equations reads as follows. Find $(p, u, h_0) \in V_p \times V_u \times \mathbb{R}$ such that for all $(q, v, w) \in V_p \times V_u \times \mathbb{R}$ there holds

$$\begin{cases} \displaystyle\int_{\Omega_c} \varepsilon(p)\nabla p \cdot \nabla q\, d\Omega - \int_{\Omega_c} \beta\rho(p) \cdot \nabla q\, d\Omega - \int_{\Omega_c} \xi p^- q\, d\Omega = 0, \\ \displaystyle\int_\Omega \mathbb{C}\epsilon_s(u) \cdot \epsilon_s(v)\, d\Omega - \int_{\Omega_c} pn \cdot v\, d\Omega = 0, \\ \displaystyle\int_{\Omega_c} pw\, d\Omega - \frac{1}{|\Omega_c|} \int_{\Omega_c} Fw\, d\Omega = 0, \end{cases}$$

where

$$V_p = \{q \in H^1(\Omega_c) : q = 0 \text{ on } \partial\Omega_c\},$$
$$V_u = \{v \in [H^1(\Omega)]^d : v = 0 \text{ on } \Omega_b\}.$$

3.3 Standard Galerkin formulation

The first approach is a standard or continuous Galerkin (CG) formulation as described in [1]. To discretize the weak form of the EHL equations of section 3.2 we start with continuous spaces for the displacement and the pressure. These spaces are defined as

$$\mathcal{V}_h := \left\{ v_h \in [C_0(\Omega)]^d : v_h|_T = \hat{v} \circ \Phi_T^{-1}, \hat{v} \in [\mathcal{P}_{k_u}(\hat{T})]^d \right\},$$
$$\mathcal{Q}_h := \left\{ q_h \in C_0(\Omega_c) : q_h|_T = \hat{q} \circ \Phi_T^{-1}, \hat{q} \in \mathcal{P}_{k_p}(\hat{T}) \right\}.$$

The displacement space $\mathcal{V}_h$ is defined on the whole domain $\Omega \subseteq \mathbb{R}^d$ while the pressure space $\mathcal{Q}_h$ is only defined on the contact area $\Omega_c \subseteq \mathbb{R}^{d-1}$. The load balance equation requires only one additional unknown which corresponds to the parameter h_0 of the film thickness equation (2.19). The full system of the EHL equations can be expressed as below.

Method 3.3.1. Find $(p_h, u_h, h_0) \in \mathcal{Q}_h \times \mathcal{V}_h \times \mathbb{R}$ such that for all $(q_h, v_h, w) \in \mathcal{Q}_h \times \mathcal{V}_h \times \mathbb{R}$ there holds

$$\begin{cases} \displaystyle\int_{\Omega_c} \varepsilon(p_h)\nabla p_h \cdot \nabla q_h \, d\Omega - \int_{\Omega_c} \beta\rho(p_h) \cdot \nabla q_h \, d\Omega = 0, \\ \displaystyle\int_{\Omega} \mathbb{C}\epsilon_s(u_h) : \epsilon_s(v_h) \, d\Omega - \int_{\Omega_c} p_h n \cdot v_h \, d\Omega = 0, \\ \displaystyle\int_{\Omega_c} p_h w_h \, d\Omega - \frac{1}{|\Omega_c|} \int_{\Omega_c} F w_h \, d\Omega = 0. \end{cases}$$

Using a continuous discretization results in oscillations for high loaded contacts. Therefore, we introduce different formulations for the EHL equations, where we focus on deriving a new formulation for the Reynolds equation as the oscillations originate from the convection dominance in the convection-diffusion like equation. In order to define the Peclet number we need to identify the convective and diffusive parts of the Reynolds equation. We recall the strong form of the Reynolds equation (2.14) and differentiate the convective term which leads to

$$\begin{aligned} &- \operatorname{div}\left(\varepsilon(p)\nabla p - \beta\rho(p)\right) = 0 \\ \Leftrightarrow &- \operatorname{div}\left(\varepsilon(p)\nabla p\right) + \beta\rho'(p) \cdot \nabla p + 12\nabla h \cdot U\rho(p) = 0. \end{aligned} \tag{3.2}$$

Now we define

$$\begin{aligned} \widetilde{\beta}(p) &:= \beta\rho'(p) = 12hU\rho'(p), \\ Q &:= 12u_m \nabla h \cdot U\rho(p), \end{aligned} \tag{3.3}$$

so the Reynolds equation reads as

$$-\operatorname{div}(\varepsilon(p)\nabla p) + \widetilde{\beta}(p)\cdot\nabla p + Q = 0.$$

Here we only defined Q to emphasize that this term has no influence on the convective-diffusive behavior of the equation. Stability problems like oscillations tend to occur for convection dominated problems. To determine this convection dominance we take a look at the Peclet number, which describes the ratio between convection and diffusion.

Definition 3.3.1. Let $\varepsilon(p)$ and $\widetilde{\beta}(p)$ be defined as in equations (2.13) and (3.3). The Peclet number of the Reynolds equation then reads as

$$\mathrm{Pe} := \frac{|\widetilde{\beta}(p)|h_{mesh}}{2k_p\varepsilon(p)}, \tag{3.4}$$

where h_{mesh} and k_p denote the mesh size and the polynomial order of the finite element space for the pressure.

For high Peclet numbers $\mathrm{Pe} > 1$ we consider a problem to be convection dominated. As mentioned before, we want to derive new formulations for the Reynolds equation such that the solution does not exhibit spurious oscillations, while the elasticity and load balance equation remain unchanged. Hence in the following sections the methods are only described for the Reynolds equation and the complete EHL system can be obtained by replacing the weak form of the Reynolds equation in Method 3.3.1 by the newly introduced formulation. Since we will consider the diffusive and convective part of the Reynolds equation separately in the following stabilized methods, we split these two parts for the continuous Galerkin formulation as well, which leads to the diffusive part

$$a^{\mathrm{CG}}(p,q) := \int_{\Omega_c} \varepsilon(p)\nabla p\cdot\nabla q\; d\Omega, \tag{3.5}$$

and the convective part

$$b^{\mathrm{CG}}(p,q) := -\int_{\Omega_c} \beta\rho(p)\cdot\nabla q\; d\Omega. \tag{3.6}$$

We will use this notation with $a(.,.)$ being the diffusive and $b(.,.)$ the convective part for all following formulations. The Reynolds equation is obtained by recombining both terms which reads as

$$\mathrm{rey}^{\mathrm{CG}}(p,q) := a^{\mathrm{CG}}(p,q) + b^{\mathrm{CG}}(p,q).$$

This is summarized in the following formulation.

Formulation 3.3.1. (Standard/Continuous Galerkin formulation)

$$\mathrm{rey}^{\mathrm{CG}}(p,q) \coloneqq \int_{\Omega_c} \varepsilon(p)\nabla p \cdot \nabla q \; d\Omega - \int_{\Omega_c} \beta\rho(p) \cdot \nabla q \; d\Omega$$

Using the above notation the weak form of the Reynolds equation can be expressed as follows.

Method 3.3.2. Find $p_h \in \mathcal{Q}_h$ such that for all $q_h \in \mathcal{Q}_h$ there holds

$$\mathrm{rey}^{\mathrm{CG}}(p_h, q_h) = 0.$$

3.4 Streamline upwind Petrov-Galerkin formulation

The first stabilization technique we consider is called streamline upwind Petrov-Galerkin (SUPG) formulation, which was introduced in [19] for general convection dominated problems and applied to the Reynolds equation in [1]. The idea is to add diffusion in streamline direction to stabilize the solution. We start from the strong form of the Reynolds equation as given in equation (2.14) and define a differential operator

$$\mathcal{L}(p) \coloneqq -\operatorname{div}\left(\varepsilon(p)\nabla p - \beta\rho(p)\right).$$

The discretized Reynolds equation in weak form then reads

$$\int_{\Omega_c} \mathcal{L}(p_h) q_h \; d\Omega = 0 \quad \forall q_h \in \mathcal{Q}_h.$$

In a more general setting one defines a differential operator $\mathcal{L}$ as done above and a right hand side f, such that the strong form $\mathcal{L}(p) = f$ holds. For the Reynolds equation we have $f = 0$, which simplifies the following considerations. The SUPG method is obtained by choosing a different test function space

$$\widetilde{\mathcal{Q}}_h \coloneqq \left\{ q_h + \alpha\widetilde{\beta}(p_h) \cdot \nabla q_h : q_h \in \mathcal{Q}_h \right\}.$$

Here α is an elementwise stabilization parameter depending on the Peclet number, which will be defined later in equation (3.8). Inserting the new test function and using equations (3.5) and (3.6) leads to

$$a^{\mathrm{CG}}(p_h, q_h) + b^{\mathrm{CG}}(p_h, q_h) + \sum_{T \in \mathcal{T}_h} \alpha \int_T \mathcal{L}(p_h) \left(\widetilde{\beta}(p_h) \cdot \nabla q_h \right) \; dx = 0 \quad \forall q_h \in \mathcal{Q}_h$$

as the weak form of the discretized Reynolds equation. Since $f = 0$, the residuum

$$\mathcal{R}(p) := f - \mathcal{L}(p) = \operatorname{div}\left(\varepsilon(p)\nabla p - \beta\rho(p)\right)$$

coincides with the negative differential operator $\mathcal{L}$. For the Reynolds equation this leads to the following expression for the residuum

$$\begin{aligned}\mathcal{R}(p) =& \operatorname{div}\left(\varepsilon(p)\nabla p - \beta\rho(p)\right) \\ =& \operatorname{div}\left(\varepsilon(p)\nabla p\right) - \beta\rho'(p)\cdot\nabla p - 12\nabla h\cdot U\rho(p) \\ =& \varepsilon(p)\Delta p + \varepsilon'(p)\nabla p\cdot\nabla p + \frac{3h^2\rho(p)}{\mu(p)}\nabla h\cdot\nabla p \\ & - \beta\rho'(p)\cdot\nabla p - 12\nabla h\cdot U\rho(p),\end{aligned} \tag{3.7}$$

where the second term

$$\varepsilon'(p) = h^3\frac{\partial}{\partial p}\left(\frac{\rho(p)}{\mu(p)}\right) = h^3\frac{\mu(p)\rho'(p) - \rho(p)\mu'(p)}{\mu(p)^2}$$

is obtained by differentiating viscosity and density with respect to the pressure. For the weak formulation of the convective term we have two choices. We can integrate by parts as for the Standard Galerkin method which leads to formulation (3.6). The second option is to differentiate the convective term of the strong form (2.14), which is done in equation (3.2). Multiplying this term with the test function results in an alternative weak form of the convective part

$$\widetilde{b}^{\mathrm{CG}}(p,q) := \int_{\Omega_c}\beta\rho'(p)\cdot\nabla pq\ d\Omega + \int_{\Omega_c}12\nabla h\cdot U\rho(p)q\ d\Omega.$$

Combining all terms we arrive at the following SUPG formulation.

Formulation 3.4.1. (Streamline upwind Petrov-Galerkin formulation)

$$\begin{aligned}\mathrm{rey}^{\mathrm{SUPG}}(p,q) :=& \int_{\Omega_c}\varepsilon(p)\nabla p\cdot\nabla q\ d\Omega \\ &+ \int_{\Omega_c}\beta\rho'(p)\cdot\nabla pq\ d\Omega \\ &+ \int_{\Omega_c}12\nabla h\cdot U\rho(p)q\ d\Omega \\ &- \sum_{T\in\mathcal{T}_h}\alpha\int_T\mathcal{R}(p)\left(\widetilde{\beta}(p)\cdot\nabla q\right)\ dx\end{aligned}$$

Here we chose the second version for the convective term as both terms already appear in the residuum. Note that the formulation is still consistent, since the residuum vanishes for the exact solution. When using the penalty method for the cavitation treatment it has to be added to the weak formulation and correspondingly to the residuum. We arrive at the following SUPG method.

Method 3.4.1. Find $p_h \in \mathcal{Q}_h$ such that for all $q_h \in \mathcal{Q}_h$ there holds

$$\mathrm{rey}^{\mathrm{SUPG}}(p_h, q_h) = 0.$$

An essential consideration in this method is selecting a suitable stabilization parameter α. A possible choice based on the elementwise Peclet number is proposed in [20]. Using the definitions from equations (3.3) and (3.4) for $\widetilde{\beta}(p)$ and Pe, respectively, we now define according to [20]

$$\alpha \coloneqq \frac{h_{\mathrm{mesh}}}{2|\widetilde{\beta}(p)|k_p}\xi(\mathrm{Pe}) \tag{3.8}$$

$$\text{with} \quad \xi(\mathrm{Pe}) = \coth(\mathrm{Pe}) - \frac{1}{\mathrm{Pe}} \quad \text{or} \quad \xi(\mathrm{Pe}) = \max\left(0, 1 - \frac{1}{\mathrm{Pe}}\right).$$

Remark. If we choose the test function space

$$\widetilde{\mathcal{Q}}_h \coloneqq \left\{ q_h + \alpha \left[\widetilde{\beta}(p_h) \cdot \nabla q_h - \mathrm{div}(\varepsilon(p_h)\nabla q_h) \right] : q_h \in \mathcal{Q}_h \right\},$$

we obtain a Galerkin least squares (GLS) formulation, which differs from the SUPG formulation by testing the residuum with $\widetilde{\beta}(p_h) \cdot \nabla q_h - \mathrm{div}(\varepsilon(p_h)\nabla q_h)$ instead of $\widetilde{\beta}(p_h) \cdot \nabla q_h$. The parameter α stays the same as for the SUPG method.

3.5 Hybrid discontinuous Galerkin formulation

Similar to the previous method, the goal is to obtain pressure solutions without spurious oscillations. Based on [21] and [2] we derive a hybridized discontinuous Galerkin method for the Reynolds equation.

3.5.1 Diffusion term

Neglecting the convective part of the Reynolds equation reduces it to the diffusive part, also known as the Poiseuille term and we obtain the equation

$$\begin{cases} -\mathrm{div}\left(\varepsilon(p)\nabla p\right) &= 0 \quad \text{in } \Omega_c, \\ p &= 0 \quad \text{on } \partial\Omega_c. \end{cases} \tag{3.9}$$

For the weak formulation we utilize discontinuous spaces, i.e. broken Sobolev spaces. Recall Definition 3.1.3, for a triangulation $\mathcal{T}_h$ of the domain Ω_c into elements $T \in \mathcal{T}_h$, the space of elementwise $H^s(T)$ functions is defined as

$$H^s(\mathcal{T}_h) := \left\{ q \in L^2(\Omega_c), q \in H^s(T) \ \forall T \in \mathcal{T}_h \right\}.$$

Since for $p \in H^1(\mathcal{T}_h)$ there no longer holds $p \in H^1(\Omega_c)$, we have to apply integration by parts for each element $T \in \mathcal{T}_h$. Hence, we obtain for $p \in H^1(\mathcal{T}_h)$ and $q \in H^1(\mathcal{T}_h)$

$$\begin{aligned} -\sum_{T\in\mathcal{T}_h} \int_T \operatorname{div}\left(\varepsilon(p)\nabla p\right) q \, dx = \sum_{T\in\mathcal{T}_h} \int_T \varepsilon(p)\nabla p \cdot \nabla q \, dx \\ - \sum_{T\in\mathcal{T}_h} \int_{\partial T} \varepsilon(p)\nabla p \cdot n \, q \, ds = 0 \end{aligned} \tag{3.10}$$

as the weak form of equation (3.9). Next we add facet functions $p_F \in L^2(\mathcal{E}_h)$ to weakly enforce continuity of the solution across elements, The Dirichlet boundary conditions for p are now applied to the facet unknowns p_F. As the normal flux $\varepsilon(p)\nabla p \cdot n$ of the exact solution is continuous, there holds

$$\sum_{T\in\mathcal{T}_h} \int_{\partial T} \varepsilon(p)\nabla p \cdot n q_F \ ds = 0 \quad \forall q_F \in L^2\left(\mathcal{E}_h\right).$$

Adding this term to the weak formulation (3.10) leads to

$$\sum_{T\in\mathcal{T}_h} \int_T \varepsilon(p)\nabla p \cdot \nabla q \ dx - \int_{\partial T} \varepsilon(p)\nabla p \cdot n(q - q_F) \ ds = 0$$

as an interim result for the weak formulation of the Poiseuille term. Since the exact solution is continuous across elements ($p - p_F = 0$ for each facet), a symmetry and a stabilization term can be added to the above equation. They are defined as

$$\begin{aligned} \sum_{T\in\mathcal{T}_h} -\int_{\partial T} \varepsilon(p)\nabla q \cdot n(p - p_F) \ ds \quad \text{(symmetry term)}, \\ \sum_{T\in\mathcal{T}_h} \int_{\partial T} \frac{\alpha^{\mathrm{HDG}} k^2}{h_{\mathrm{mesh}}} (p - p_F)(q - q_F) \ ds \quad \text{(stabilization term)}. \end{aligned}$$

The constant α^{HDG} has to be chosen large enough to obtain coercivity for the resulting bilinearform. In the coercivity proof with $\varepsilon(p)$ being constant, the factors k^2 and h_{mesh} arise from the inverse inequality for polynomials. Even though $\varepsilon(p)$ is

not constant in our case, we keep this scaling for the stabilization term. Combining all terms leads to the following formulation of the Poiseuille term

$$\begin{aligned} a^{\mathrm{HDG}}\left((p,p_F),(q,q_F)\right) := & \sum_{T\in\mathcal{T}_h}\int_T \varepsilon(p)\nabla p\cdot\nabla q\ dx \\ & - \sum_{T\in\mathcal{T}_h}\int_{\partial T} \varepsilon(p)\nabla p\cdot n\,(q-q_F)\ \ dx \\ & - \sum_{T\in\mathcal{T}_h}\int_{\partial T} \varepsilon(p)\nabla q\cdot n\,(p-p_F)\ \ dx \\ & + \frac{\alpha^{\mathrm{HDG}}k^2}{h_{\mathrm{mesh}}}\sum_{T\in\mathcal{T}_h}\int_{\partial T}\varepsilon(p)\,(p-p_F)\,(q-q_F)\ \ dx. \end{aligned}$$

3.5.2 Convection term

Similar to the previous section we now only consider the convective part of the Reynolds equation and assume the diffusive part to be zero. The convective term, also known as the Couette term, reads as

$$\begin{cases} \mathrm{div}\left(\beta\rho(p)\right) &= 0 \quad \text{in } \Omega_c, \\ p &= 0 \quad \text{on } \partial\Omega_c. \end{cases} \tag{3.11}$$

Based on [2] we derive a HDG formulation for the Couette term of the Reynolds equation. Again we start with integration by parts on each element $T \in \mathcal{T}_h$, which leads to

$$\begin{aligned} \sum_{T\in\mathcal{T}_h}\int_T \mathrm{div}\left(\beta\rho(p)\right)q\,dx = & \sum_{T\in\mathcal{T}_h} -\int_T \beta\rho(p)\cdot\nabla q\,dx \\ & + \sum_{T\in\mathcal{T}_h}\int_{\partial T}\beta\cdot n\,\rho(p)q\,ds = 0, \end{aligned} \tag{3.12}$$

being the weak form of equation (3.11). The boundary integrals are now adjusted by inserting the upwind value p^{up} instead of p. For this purpose we define the inflow and outflow boundary of each element T.

Definition 3.5.1. (Inflow and outflow boundary) Let $T \in \mathcal{T}_h$ be an element of the triangulation and ∂T its boundary. The inflow and outflow boundary are defined as

$$\begin{aligned} \partial T_{out} &:= \{x \in \partial T : \beta \cdot n > 0\}, \\ \partial T_{in} &:= \{x \in \partial T : \beta \cdot n \leq 0\} = \partial T \setminus \partial T_{out}. \end{aligned}$$

Using these definitions we can now define the upwind value.

Definition 3.5.2. (Upwind value - Standard) Let $p \in H^s(\mathcal{T}_h)$ and $p_F \in L^2(\mathcal{E}_h)$ then the upwind value p^{up} is defined as

$$p^{up} = \begin{cases} p, & \partial T_{out}, \\ p_F, & \partial T_{in}. \end{cases}$$

Note that usually β is required to be divergence free, which is not the case for the Reynolds equation. Therefore, we consider different approaches for the upwind value based on the derivative of the Couette term and the linearization of the full Reynolds equation.

Definition 3.5.3. (Upwind value - Couette derivative)

$$p^{up} = \begin{cases} p, & \beta\rho'(p) \cdot n > 0, \\ p_F, & \beta\rho'(p) \cdot n \leq 0. \end{cases}$$

Another suitable choice for the upwind value can be obtained by linearizing the Reynolds equation and not only the Couette term, since $\varepsilon(p)$ is not constant. Hence we differentiate the terms of Formulation 3.3.1 with respect to the pressure p, which leads to

$$\begin{aligned} \frac{\partial}{\partial p}\left(\varepsilon(p)\nabla p \cdot \nabla q - \beta\rho(p) \cdot \nabla q\right)|_{p=\widetilde{p}} &= \varepsilon(\widetilde{p})\nabla q \cdot \nabla(.) + \varepsilon'(\widetilde{p})\nabla\widetilde{p} \cdot \nabla q \\ &\quad - \beta\rho'(\widetilde{p}) \cdot \nabla q \end{aligned}$$

for the previous guess $\widetilde{p}$. Using the convective terms

$$(\beta\rho'(\widetilde{p}) - \varepsilon'(\widetilde{p})\nabla\widetilde{p}) \cdot \nabla q$$

from the above linearization, we now define a third version of the upwind value.

Definition 3.5.4. (Upwind value - Full linearization)

$$p^{up} = \begin{cases} p, & (\beta\rho'(p) - \varepsilon'(p)\nabla p) \cdot n > 0, \\ p_F, & (\beta\rho'(p) - \varepsilon'(p)\nabla p) \cdot n \leq 0. \end{cases}$$

Recalling the weak formulation (3.12) we now replace p by p^{up} in the boundary integral with one of the above definitions, resulting in

$$\sum_{T\in\mathcal{T}_h} \int_T \operatorname{div}(\beta\rho(p))\, q \, dx = \sum_{T\in\mathcal{T}_h} -\int_T \beta\rho(p)\cdot\nabla q \, dx \tag{3.13}$$

$$+ \sum_{T\in\mathcal{T}_h} \int_{\partial T} \beta\cdot n\rho(p^{up}) q \, ds = 0 \tag{3.14}$$

as the weak form of equation (3.11) with upwinding. This leads to a decoupling of the elements. The outflow edges do not couple with the facet unknowns anymore. To reintroduce this coupling we add the term

$$\sum_{T\in\mathcal{T}_h} \int_{\partial T_{out}} \beta\cdot n\left[\rho(p_F) - \rho(p)\right] q_F \, ds$$

for the outflow edges, which vanishes for the exact solution, since $p_F = p$ on the facets. Combining all terms leads to

$$\begin{aligned} b^{\mathrm{HDG}}\left((p,p_F),(q,q_F)\right) := &- \sum_{T\in\mathcal{T}_h} \int_T \beta\rho(p)\cdot\nabla q \, dx \\ &+ \sum_{T\in\mathcal{T}_h} \int_{\partial T} \beta\cdot n\rho\left(p^{up}\right) q \, ds \\ &+ \sum_{T\in\mathcal{T}_h} \int_{\partial T_{out}} \beta\cdot n\left[\rho(p_F) - \rho(p)\right] q_F \, ds, \end{aligned} \tag{3.15}$$

being the formulation of the Couette term. An equivalent but more compact formulation is given by

$$\begin{aligned} b^{\mathrm{HDG}}\left((p,p_F),(q,q_F)\right) = &- \sum_{T\in\mathcal{T}_h} \int_T \beta\rho(p)\cdot\nabla q \, dx \\ &- \sum_{T\in\mathcal{T}_h} \int_{\partial T} \beta\cdot n\rho\left(p^{up}\right)\left(q_F - q\right) ds. \end{aligned} \tag{3.16}$$

Here we used that

$$-\sum_{T\in\mathcal{T}_h}\int_{\partial T}\beta\cdot n\rho(p^{up})\,(q_F-q)\;\,ds=\sum_{T\in\mathcal{T}_h}\int_{\partial T}\beta\cdot n\rho(p^{up})q\;ds \\ -\sum_{T\in\mathcal{T}_h}\int_{\partial T}\beta\cdot n\rho(p^{up})q_F\;ds,$$

and considering the second term on the right hand side we obtain

$$\begin{aligned}
&-\sum_{T\in\mathcal{T}_h}\int_{\partial T}\beta\cdot n\,\rho(p^{up})q_F\;ds= \\
&\quad=-\sum_{T\in\mathcal{T}_h}\int_{\partial T_{in}}\beta\cdot n\,\rho(p_F)q_F\;ds-\sum_{T\in\mathcal{T}_h}\int_{\partial T_{out}}\beta\cdot n\,\rho(p)q_F\;ds \\
&\quad=\sum_{T\in\mathcal{T}_h}\int_{\partial T_{out}}\beta\cdot n\;\left[\rho(p_F)-\rho(p)\right]q_F\;ds \\
&\qquad-\int_{\partial T\cap\Gamma}\beta\cdot n\,\rho(p_F)q_F\;ds.
\end{aligned}$$

The first equality holds, since the common edge of two neighboring elements is considered as outflow edge for one element and as inflow edge for the other element. Therefore, when using the upwind value as in the first expression we end up with the difference of the facet and the element value for each edge. The facet value originates from the inflow and the element value from the outflow edge. The sign of the inflow term changes since the normal vector of the edge on the inflow boundary points in the opposite direction compared to the outflow boundary. For the boundary of the domain the edges are either inflow or outflow edges, therefore, we have to add the last term, which vanishes for homogeneous Dirichlet boundary conditions.

Stabilization term for convection

Using the work of [21] and [22], where a mixed formulation for linear and nonlinear convection-diffusion equations is considered, we obtain a similar formulation for the convective part of the Reynolds equation. However, this formulation is not solely based on upwinding, but more general stabilization strategies, e.g. a Lax like approach. Instead of replacing the pressure p by the upwind value p^{up} in the boundary integral of equation (3.12), a numerical flux $\hat{p}$ is used. The numerical flux $\hat{p}$ can be defined as function of facet and element unknowns. Neglecting the

diffusion part, the mentioned works lead to

$$\begin{aligned}\hat{b}^{\mathrm{HDG}}\left((p,\hat{p}),(q,\hat{q})\right) := &-\sum_{T\in\mathcal{T}_h}\int_T \beta\rho(p)\cdot\nabla q\ dx \\ &-\sum_{T\in\mathcal{T}_h}\int_{\partial T}\beta\cdot n\rho\left(\hat{p}\right)\left(\hat{q}-q\right)\ ds \\ &+\sum_{T\in\mathcal{T}_h}\int_{\partial T}\tau(p-\hat{p})(q-\hat{q})\ ds\end{aligned} \tag{3.17}$$

as formulation of the convection term, where $\hat{q}$ is the test function corresponding to the numerical flux $\hat{p}$ and τ is a stabilization parameter. According to [21] and [23] a reasonable choice for this stabilization parameter is given by

$$\tau = \frac{1}{2}\left(\max\left\{\left|\beta\cdot n\rho'(p)\right|,\left|\beta\cdot n\rho'(p_F)\right|\right\}\right).$$

Comparing equations (3.16) and (3.17) and choosing $\hat{p}=p^{up}, \hat{q}=q_F$ leads to

$$\hat{b}^{\mathrm{HDG}}\left((p,p^{up}),(q,q_F)\right) = b^{\mathrm{HDG}}\left((p,p_F),(q,q_F)\right) + \sum_{T\in\mathcal{T}_h}\int_{\partial T}\tau(p-p^{up})(q-q_F)\ ds,$$

which means that both formulations result in the same weak form up to a stabilization term when using the upwind value.

3.5.3 Convection-diffusion problem

The HDG formulation of the Reynolds equation using mass-conserving cavitation treatment is obtained by replacing $\rho(p)$ by $\rho_0(p)f(p)$ in the formulation of the Couette term (3.15). This results in

$$\begin{aligned}b^{\mathrm{HDG}}\left((p,p_F),(q,q_F)\right) := &-\sum_{T\in\mathcal{T}_h}\int_T \beta f(p)\rho_0(p)\cdot\nabla q\ dx \\ &+\sum_{T\in\mathcal{T}_h}\int_{\partial T}\beta\cdot n f(p^{up})\rho_0(p^{up})q\ ds \\ &+\sum_{T\in\mathcal{T}_h}\int_{\partial T_{out}}\beta\cdot n\left[f(p_F)\rho_0(p_F)-f(p)\rho_0(p)\right]q_F\ ds\end{aligned}$$

being the final formulation of the convection term. The diffusion term does not change as the density and viscosity appear in $\varepsilon(p)$ in the numerator and the denominator, thus, the function $f(p)$ cancels out. Combining both terms we obtain

$$\mathrm{rey}^{\mathrm{HDG}}\left((p,p_F),(q,q_F)\right) := a^{\mathrm{HDG}}\left((p,p_F),(q,q_F)\right) + b^{\mathrm{HDG}}\left((p,p_F),(q,q_F)\right)$$

as the HDG formulation of the Reynolds equation.

Formulation 3.5.1. (Hybrid discontinuous Galerkin formulation)

$$\begin{aligned}
\mathrm{rey}^{\mathrm{HDG}}\left((p,p_F),(q,q_F)\right) := & \sum_{T\in\mathcal{T}_h}\int_T \varepsilon(p)\nabla p\cdot\nabla q\ dx \\
& -\sum_{T\in\mathcal{T}_h}\int_{\partial T}\varepsilon(p)\nabla p\cdot n\,(q-q_F)\ dx \\
& -\sum_{T\in\mathcal{T}_h}\int_{\partial T}\varepsilon(p)\nabla q\cdot n\,(p-p_F)\ dx \\
& -\sum_{T\in\mathcal{T}_h}\int_T \beta f(p)\rho_0(p)\cdot\nabla q\ dx \\
& +\sum_{T\in\mathcal{T}_h}\int_{\partial T}\beta\cdot n f(p^{up})\rho_0(p^{up})q\ ds \\
& +\sum_{T\in\mathcal{T}_h}\int_{\partial T_{out}}\beta\cdot n\left[f(p_F)\rho_0(p_F)-f(p)\rho_0(p)\right]q_F\ ds \\
& +\frac{\alpha^{\mathrm{HDG}}k^2}{h_{\mathrm{mesh}}}\sum_{T\in\mathcal{T}_h}\int_{\partial T}\varepsilon(p)\,(p-p_F)\,(q-q_F)\ dx
\end{aligned}$$

Using the notation from above and defining the discretization spaces as

$$\begin{aligned}
\mathcal{Q}_h &:= \left\{q_h\in L^2(\Omega_c):\ q_h|_T=\hat{q}\circ\Phi_T^{-1},\hat{q}\in\mathcal{P}_k(\hat{T})\right\},\\
\mathcal{M}_h &:= \left\{\mu_h\in L^2\left(\mathcal{E}_h\right):\ \mu_h|_E=\hat{\mu}\circ\Phi_E^{-1},\mu_h=0\text{ on }\partial\Omega_c,\hat{\mu}\in\mathcal{P}_k(\hat{E})\right\},
\end{aligned}$$

we arrive at the following HDG method.

Method 3.5.1. Find $(p_h,p_{F,h})\in\mathcal{Q}_h\times\mathcal{M}_h$ such that for all $q_h\in\mathcal{Q}_h$ and $q_{F,h}\in\mathcal{M}_h$ there holds

$$\mathrm{rey}^{\mathrm{HDG}}\left((p_h,p_{F,h}),(q_h,q_{F,h})\right)=0.$$

3.6 Two-field mixed formulation

Another approach similar to the HDG formulation is a hybridized mixed formulation as proposed in [3]. The main advantage of a mixed formulation compared to the previously discussed methods is, that it does not require a stabilization parameter, which had to be chosen in either of the previous methods. We now

enforce normal continuity of the flux via constraints for the newly introduced flux field

$$\sigma = -\varepsilon(p)\nabla p. \tag{3.18}$$

The Reynolds equation reads

$$\begin{cases} \operatorname{div}(\sigma + \beta\rho(p)) &= 0 \quad \text{in } \Omega_c, \\ p &= 0 \quad \text{on } \partial\Omega_c. \end{cases} \tag{3.19}$$

For readability purposes we define the notations

$$(.,.)_{\mathcal{T}_h} := \sum_{T\in\mathcal{T}_h} \int_T (.)\, dx \quad \text{and} \quad \langle .,. \rangle_{\partial\mathcal{T}_h} := \sum_{T\in\mathcal{T}_h} \int_{\partial T} (.)\, ds$$

for the inner products. The discretization spaces for the pressure and facet unknowns are the same as for the HDG method. For the discretization of the flux we use the Raviart-Thomas (-Nedelec) element [24], resulting in the following spaces

$$\begin{aligned} \Sigma_h &:= \left\{ \tau_h \in \left[L^2(\Omega_c)\right]^d : \tau_h|_T = \frac{1}{\det \Phi_T'} \Phi_T' \hat{\tau} \circ \Phi_T^{-1}, \hat{\tau} \in \mathcal{P}_k(\hat{T}) \oplus \vec{x} \cdot \mathcal{P}_k(\hat{T}) \right\}, \\ \mathcal{Q}_h &:= \left\{ q_h \in L^2(\Omega_c) : q_h|_T = \hat{q} \circ \Phi_T^{-1}, \hat{q} \in \mathcal{P}_k(\hat{T}) \right\}, \\ \mathcal{M}_h &:= \left\{ \mu_h \in L^2(\mathcal{E}_h) : \mu_h|_E = \hat{\mu} \circ \Phi_E^{-1}, \mu_h = 0 \text{ on } \partial\Omega_c, \hat{\mu} \in \mathcal{P}_k(\hat{E}) \right\}, \end{aligned}$$

where $\oplus$ denotes the union of two vector spaces. As for the HDG method we start by deriving formulations for the diffusive and convective part seperately.

3.6.1 Diffusion term

Considering only the Poiseuille term the Reynolds equation reduces to

$$\sigma = -\varepsilon(p)\nabla p, \quad \operatorname{div}\sigma = 0 \quad \text{in } \Omega_c, \quad p = 0 \quad \text{on } \partial\Omega_c. \tag{3.20}$$

Breaking the continuity between the elements leads to

$$\begin{aligned} \left(\frac{1}{\varepsilon(p)}\sigma, \tau\right)_{\mathcal{T}_h} + (\nabla p, \tau)_{\mathcal{T}_h} &= 0 \quad \forall \tau \in \left[H^1(\mathcal{T}_h)\right]^d, \\ (\sigma, \nabla q)_{\mathcal{T}_h} + \langle -\sigma \cdot n, q \rangle_{\partial\mathcal{T}_h} &= 0 \quad \forall q \in H^1(\mathcal{T}_h), \end{aligned}$$

as mixed formulation in weak form, where τ is the test function associated to the new field and q is the test function for the pressure space. Similar to section 3.5.1 we add consistent terms

$$\begin{aligned} \langle \sigma \cdot n, q_F \rangle_{\partial\mathcal{T}_h} &= 0, \\ \langle p_F - p, \tau \cdot n \rangle_{\partial\mathcal{T}_h} &= 0 \end{aligned}$$

to the equations. The first term amounts to zero since the exact flux solution σ is normal continuous. The second equation holds as the solution p itself is continuous. So we end up with

$$a^{\mathrm{HM2F}}\left((\sigma,p,p_F),(\tau,q,q_F)\right) := \left(\frac{1}{\varepsilon(p)}\sigma,\tau\right)_{\mathcal{T}_h} + (\nabla p,\tau)_{\mathcal{T}_h} + (\sigma,\nabla q)_{\mathcal{T}_h} + \langle\sigma\cdot n, q_F - q\rangle_{\partial\mathcal{T}_h} + \langle p_F - p, \tau\cdot n\rangle_{\partial\mathcal{T}_h}$$

as formulation of the diffusion term.

3.6.2 Convection term

Since the flux variable σ only appears in the diffusion part of the Reynolds equation, the convective part remains unchanged compared to the HDG formulation. The equation

$$\mathrm{div}\left(\beta\rho(p)\right) = 0 \quad \text{in } \Omega_c, \quad p = 0 \quad \text{on } \partial\Omega_c \tag{3.21}$$

leads to the weak formulation

$$(\rho(p),\beta\cdot\nabla q)_{\mathcal{T}_h} - \langle\beta\cdot n\rho(p^{up}),q\rangle_{\partial\mathcal{T}_h} = 0,$$

if we break continuity and apply upwinding. Similar to section 3.5.2 we add a term to reintroduce coupling on the outflow edges, resulting in

$$b^{\mathrm{HM}}\left((p,p_F),(q,q_F)\right) := (\rho(p),\beta\cdot\nabla q)_{\mathcal{T}_h} + \langle\beta\cdot n\rho(p^{up}),q_F - q\rangle_{\partial\mathcal{T}_h}.$$

The choice of the upwind value p^{up} is the same as for the HDG method. Note that here we used the more compact formulation for recoupling of the outflow edges with the facet variables.

3.6.3 Convection-diffusion problem

Using the work from the previous sections and combining the diffusion and convection terms leads to the weak formulation

$$\mathrm{rey}^{\mathrm{HM2F}}\left((\sigma,p,p_F),(\tau,q,q_F)\right) := a^{\mathrm{HM2F}}\left((\sigma,p,p_F),(\tau,q,q_F)\right) + b^{\mathrm{HM}}\left((p,p_F),(q,q_F)\right).$$

Collecting all the terms, we obtain

$$\begin{aligned}\mathrm{rey}^{\mathrm{HM2F}}\left((\sigma,p,p_F),(\tau,q,q_F)\right) := {} & \left(\frac{1}{\varepsilon(p)}\sigma,\tau\right)_{\mathcal{T}_h} + (\nabla p,\tau)_{\mathcal{T}_h} \\ & + (\sigma,\nabla q)_{\mathcal{T}_h} + \langle\sigma\cdot n, q_F - q\rangle_{\partial\mathcal{T}_h} \\ & + \langle p_F - p,\tau\cdot n\rangle_{\partial\mathcal{T}_h} \\ & + (\rho(p),\beta\cdot\nabla q)_{\mathcal{T}_h} + \langle\beta\cdot n\rho(p^{up}),q_F - q\rangle_{\partial\mathcal{T}_h}\end{aligned}$$

as the two-field mixed formulation of the Reynolds equation. The issue with this two-field formulation is, that the term $\varepsilon(p)$ appears in the denominator of the diffusive part. As $\varepsilon(p)$ becomes small for high pressures due to the increasing viscosity, this term leads to numerical instabilities. To overcome this issue we introduce a third field in the next section.

3.7 Three-field mixed formulation

The formulation of the convective part stays the same as for the two-field mixed formulation, hence we only consider the diffusive part of the Reynolds equation. We start from the set of equations

$$g := -\nabla p, \quad \sigma = \varepsilon(p)\nabla p, \quad \operatorname{div}\sigma = 0 \quad \text{in } \Omega_c, \quad p = 0 \quad \text{on } \partial\Omega_c \tag{3.22}$$

or in a different, equivalent way

$$g = -\frac{1}{\varepsilon(p)}\sigma, \quad \sigma = \varepsilon(p)\nabla p, \quad \operatorname{div}\sigma = 0 \quad \text{in } \Omega_c, \quad p = 0 \quad \text{on } \partial\Omega_c.$$

Using the equations from the two field formulation

$$\begin{aligned} \left(-\frac{1}{\varepsilon(p)}\sigma, \tau\right)_{\mathcal{T}_h} + (\nabla p, \tau)_{\mathcal{T}_h} = 0 \quad \forall \tau \in \left[H^1(\mathcal{T}_h)\right]^d, \\ (\sigma, \nabla q)_{\mathcal{T}_h} + \langle -\sigma \cdot n, q\rangle_{\partial\mathcal{T}_h} = 0 \quad \forall q \in H^1(\mathcal{T}_h) \end{aligned}$$

and inserting the new variable g leads to

$$\begin{aligned} (g, \tau)_{\mathcal{T}_h} + (\nabla p, \tau)_{\mathcal{T}_h} = 0 \quad \forall \tau \in \left[H^1(\mathcal{T}_h)\right]^d, \\ (\sigma, \tilde{g})_{\mathcal{T}_h} + (\varepsilon(p) g, \tilde{g})_{\mathcal{T}_h} = 0 \quad \forall \tilde{g} \in \left[H^1(\mathcal{T}_h)\right]^d, \\ (\sigma, \nabla q)_{\mathcal{T}_h} + \langle -\sigma \cdot n, q\rangle_{\partial\mathcal{T}_h} = 0 \quad \forall q \in H^1(\mathcal{T}_h). \end{aligned}$$

We add the same consistent terms as in the two-field formulation

$$\begin{aligned} \langle \sigma \cdot n, q_F\rangle_{\partial\mathcal{T}_h} = 0, \\ \langle p_F - p, \tau \cdot n\rangle_{\partial\mathcal{T}_h} = 0, \end{aligned}$$

which results in

$$\begin{aligned} a^{\mathrm{HM3F}}\left((\sigma, g, p, p_F), (\tau, \tilde{g}, q, q_F)\right) := (g, \tau)_{\mathcal{T}_h} + (\nabla p, \tau)_{\mathcal{T}_h} + (\sigma, \nabla q)_{\mathcal{T}_h} \\ + (\sigma, \tilde{g})_{\mathcal{T}_h} + (\varepsilon(p) g, \tilde{g})_{\mathcal{T}_h} \\ + \langle \sigma \cdot n, q_F - q\rangle_{\partial\mathcal{T}_h} + \langle p_F - p, \tau \cdot n\rangle_{\partial\mathcal{T}_h} \end{aligned}$$

as formulation of the diffusion term. Adding the convection term from the previous section leads to

$$\begin{aligned}\mathrm{rey}^{\mathrm{HM3F}}\left((\sigma,g,p,p_F),(\tau,\tilde{g},q,q_F)\right) := a^{\mathrm{HM3F}}\left((\sigma,g,p,p_F),(\tau,\tilde{g},q,q_F)\right)\\ + b^{\mathrm{HM}}\left((p,p_F),(q,q_F)\right),\end{aligned}$$

or in a more expanded form

$$\begin{aligned}\mathrm{rey}^{\mathrm{HM3F}}\left((\sigma,g,p,p_F),(\tau,\tilde{g},q,q_F)\right) := {}& (g,\tau)_{\mathcal{T}_h} + (\nabla p,\tau)_{\mathcal{T}_h} + (\sigma,\nabla q)_{\mathcal{T}_h}\\ &+ (\sigma,\tilde{g})_{\mathcal{T}_h} + (\varepsilon(p)g,\tilde{g})_{\mathcal{T}_h}\\ &+ \langle\sigma\cdot n, q_F - q\rangle_{\partial\mathcal{T}_h} + \langle p_F - p, \tau\cdot n\rangle_{\partial\mathcal{T}_h}\\ &+ (\rho(p),\beta\cdot\nabla q)_{\mathcal{T}_h} + \langle\beta\cdot n\rho(p^{up}), q_F - q\rangle_{\partial\mathcal{T}_h}\end{aligned}$$

being the three-field mixed formulation of the Reynolds equation. Similar to the HDG formulation, we alter viscosity and density with a function $f(p)$ to ensure pressure positivity.

Formulation 3.7.1. (Hybrid mixed three-field discontinuous Galerkin formulation)

$$\begin{aligned}&\mathrm{rey}^{\mathrm{HM3F}}\left((\sigma,g,p,p_F),(\tau,\tilde{g},q,q_F)\right) :=\\ &\sum_{T\in\mathcal{T}_h}\int_T \sigma\cdot\nabla q\ dx - \sum_{T\in\mathcal{T}_h}\int_T \beta f(p)\rho_0(p)\cdot\nabla q\ dx\\ &+\sum_{T\in\mathcal{T}_h}\int_{\partial T}\sigma\cdot n\,(q_F - q)\ ds - \sum_{T\in\mathcal{T}_h}\int_{\partial T}\beta\cdot n f(p^{up})\rho_0(p^{up})\,(q_F - q)\ ds\\ &+\sum_{T\in\mathcal{T}_h}\int_T \nabla p\cdot\tau\ dx + \sum_{T\in\mathcal{T}_h}\int_T g\cdot\tau\ dx\\ &+\sum_{T\in\mathcal{T}_h}\int_T \sigma\cdot\tilde{g}\ dx + \sum_{T\in\mathcal{T}_h}\int_T \varepsilon(p)g\cdot\tilde{g}\ dx\\ &+\sum_{T\in\mathcal{T}_h}\int_{\partial T}(p_F - p)\tau\cdot n\ ds\end{aligned}$$

We arrive at the following three-field mixed method.

Method 3.7.1. Find $(\sigma_h, g_h, p_h, p_{F,h}) \in \Sigma_h \times \Sigma_h \times \mathcal{Q}_h \times \mathcal{M}_h$ such that for all $\tau_h \in \Sigma_h$, $\tilde{g} \in \Sigma_h$, $q_h \in \mathcal{Q}_h$, $q_{F,h} \in \mathcal{M}_h$ there holds

$$\text{rey}^{\text{HM3F}}\left((\sigma_h, g_h, p_h, p_{F,h}), (\tau_h, \tilde{g}, q_h, q_{F,h})\right) = 0.$$

As mentioned before, one main advantage of the mixed formulation compared to the HDG method is the natural stabilization via the flux variable. Thus no stabilization parameter has to be chosen. Furthermore the flux variable can be used to recover one order for the pressure variable as shown in [3].

3.7.1 Postprocessing of the scalar variable

Let $(\sigma_h, g_h, p_h, p_{F,h}) \in \Sigma_h \times \Sigma_h \times \mathcal{Q}_h \times \mathcal{M}_h$ be the solution of the three-field mixed method. We now define the spaces

$$\widetilde{\mathcal{Q}_h} := \left\{ q_h \in L_2(\Omega_c) : q_h|_T = \hat{q} \circ \Phi_T^{-1}, \hat{q} \in \mathcal{P}_{k+1}(\hat{T}) \right\},$$
$$\Lambda_h := \left\{ q_h \in L_2(\Omega_c) : q_h|_T = \hat{q} \circ \Phi_T^{-1}, \hat{q} \in \mathcal{P}_0(\hat{T}) \right\}$$

and $(\widetilde{p_h}, \lambda_h) \in \widetilde{\mathcal{Q}_h} \times \Lambda_h$ as the solution of the variational problem

$$\begin{aligned} (\varepsilon(p_h)\widetilde{p_h}, \nabla q_h)_{\mathcal{T}_h} + (\lambda_h, q_h)_{\mathcal{T}_h} &= (\sigma_h, \nabla q_h)_{\mathcal{T}_h} \quad \forall q_h \in \widetilde{\mathcal{Q}_h}, \\ (\widetilde{p_h}, \mu_h)_{\mathcal{T}_h} &= (p_h, \mu_h)_{\mathcal{T}_h} \quad \forall \mu_h \in \Lambda_h, \end{aligned}$$

where λ_h is a Lagrange multiplier. Note that for the three field mixed formulation we introduced two flux variables σ_h and g_h, either one of them can be used for postprocessing. Using g_h instead of σ_h leads to the variational problem

$$\begin{aligned} (\widetilde{p_h}, \nabla q_h)_{\mathcal{T}_h} + (\lambda_h, q_h)_{\mathcal{T}_h} &= -(g_h, \nabla q_h)_{\mathcal{T}_h} \quad \forall q_h \in \widetilde{\mathcal{Q}_h}, \\ (\widetilde{p_h}, \mu_h)_{\mathcal{T}_h} &= (p_h, \mu_h)_{\mathcal{T}_h} \quad \forall \mu_h \in \Lambda_h. \end{aligned}$$

3.8 Isotropic diffusion

For line contact problems (2d) the stabilized methods show no oscillatory behavior as shown in section 4.2. However for circular contact problems (3d) the stabilization only leads to damped oscillations. This can be seen in section 4.3. To overcome this issue, we introduce an additional isotropic diffusion term to the Reynolds equation as proposed in [1]. Therefore, we define

$$a_{\text{CG}}^{\text{ID}}(p, q) := \sum_{T \in \mathcal{T}_h} \rho_{\text{id}} \frac{h_{\text{mesh}} |\widetilde{\beta}|}{2k} \nabla p \cdot \nabla q \, dx, \tag{3.23}$$

where ρ_{id} is a parameter which should be chosen as small as possible since it alters the original problem. Recalling the derivation of the HDG method for the diffusive part, we include the facet terms as well, which leads to

$$\begin{aligned} a_{\mathrm{HDG}}^{\mathrm{ID}}\left((p,p_F),(q,q_F)\right) := & \sum_{T\in\mathcal{T}_h}\int_T \rho_{\mathrm{id}}\frac{h_{\mathrm{mesh}}|\widetilde{\beta}|}{2k}\nabla p\cdot\nabla q\ dx \\ & -\sum_{T\in\mathcal{T}_h}\int_{\partial T}\rho_{\mathrm{id}}\frac{h_{\mathrm{mesh}}|\widetilde{\beta}|}{2k}\nabla p\cdot n\,(q-q_F)\ dx \\ & -\sum_{T\in\mathcal{T}_h}\int_{\partial T}\rho_{\mathrm{id}}\frac{h_{\mathrm{mesh}}|\widetilde{\beta}|}{2k}\nabla q\cdot n\,(p-p_F)\ dx \\ & +\frac{1}{2}\alpha^{\mathrm{HDG}}k\sum_{T\in\mathcal{T}_h}\int_{\partial T}\rho_{\mathrm{id}}|\widetilde{\beta}|\,(p-p_F)\,(q-q_F)\ dx \end{aligned} \tag{3.24}$$

as an isotropic diffusion term for the HDG method. Here we cancelled out h_{mesh} and k of the stabilization term with the ones arising from the isotropic diffusion term. To include isotropic diffusion in the formulations of the Reynolds equation, we add the respective term to the original formulation.

Chapter 4

Comparison of the formulations

In this chapter the presented formulations are compared regarding accuracy and efficiency. As initial benchmark we consider a convection-diffusion problem with known analytic solution as done in [2, 3]. In sections 4.2 and 4.3 we consider line and circular contact problems, which are standard test cases in elastohydrodynamic lubrication simulations. The results are compared to the ones presented in [1]. As a more complex test case we consider a block on ring problem in section 4.4, where both bodies are meshed and the film thickness is calculated via the distance of the surfaces instead of using an analytic expression. This approach is more flexible and can be applied to arbitrary geometries. All computations are performed using the finite element library Netgen/NGSolve [25]. The simulations are executed on a system equipped with an AMD Ryzen 7 5700G (3.8 GHz) processor, 32 GB RAM and 16 shared memory cores.

4.1 Convection-diffusion problem

We consider a convection-diffusion problem on the unit square $\Omega = (0,1)^2$ with constant coefficients $\varepsilon = 0.01$ and $\beta = (2,1)^T$, which reads as

$$\begin{aligned} -\varepsilon \Delta u + \beta \cdot \nabla u &= f \quad \text{in } \Omega, \\ u &= 0 \quad \text{on } \partial\Omega. \end{aligned} \tag{4.1}$$

The source term f is chosen as

$$f(x,y) = \beta_1 \left(y - \frac{\exp(\beta_2 y/\varepsilon) - 1}{\exp(\beta_2/\varepsilon) - 1} \right) + \beta_2 \left(x - \frac{\exp(\beta_1 x/\varepsilon) - 1}{\exp(\beta_1/\varepsilon) - 1} \right),$$

such that the analytic solution is given by

$$u(x,y) = \left(x - \frac{\exp(\beta_1 x/\varepsilon) - 1}{\exp(\beta_1/\varepsilon) - 1} \right) \left(y - \frac{\exp(\beta_2 y/\varepsilon) - 1}{\exp(\beta_2/\varepsilon) - 1} \right).$$

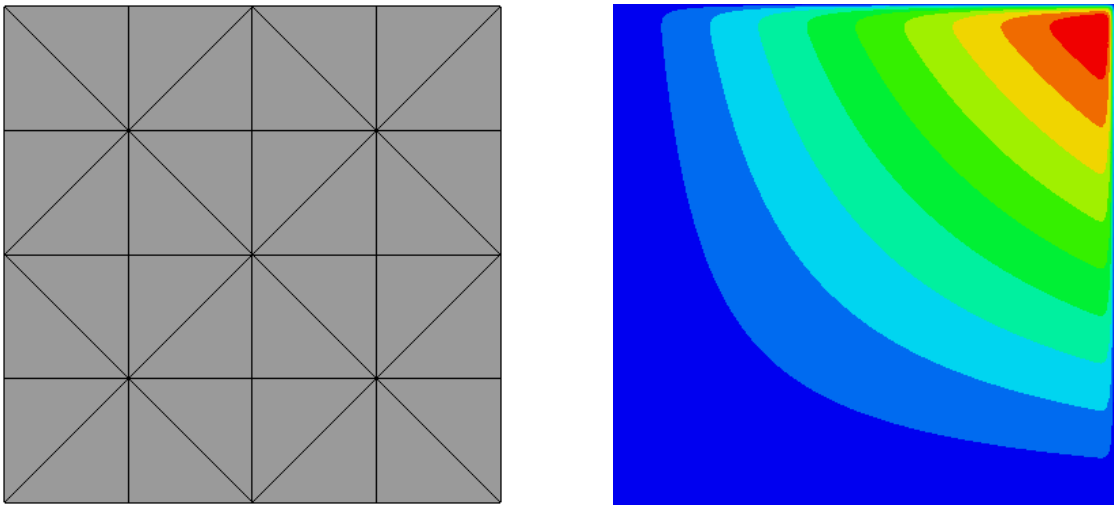

(a) Initial mesh ($L = 0$) **(b)** CG solution ($L = 3$, $k = 2$)

Figure 4.1: Convection-diffusion problem: Initial mesh and CG solution

The problem is solved using the CG, SUPG, GLS (see Remark 3.4), HDG and two-field mixed formulation for polynomial degrees $k = 1, 2, 3$ on a sequence of uniformly refined meshes with refinement levels $L = 0, 1, 2, 3$. The L^2-errors are computed (see Table 4.1) and the computation time is measured for each method (see Table 4.2). Since $\varepsilon = 0.01$ and $\beta = (2, 1)^T$ are constant the residuum of equation (4.1) reads

$$R(u_h) = f - \beta \cdot \nabla u_h + \varepsilon \Delta u_h.$$

The stabilization parameter for the SUPG and GLS method is chosen according to equation (3.8) with $\widetilde{\beta} = \beta$. For the mixed method the L^2-errors are computed using the postprocessed solution as described in section 3.7.1. The initial mesh and an example solution created with the CG approach for level $L = 3$ and polynomial order $k = 2$ are depicted in Figure 4.1.

Level	Elements	CG		SUPG		GLS		HDG		Mixed	
		k=1	k=2	k=1	k=2	k=1	k=2	k=1	k=2	k=0	k=1
L=0	32	1.11	0.34	0.18	0.12	0.18	0.12	0.028	0.035	0.078	0.031
L=1	128	0.30	0.10	0.12	0.066	0.12	0.065	0.026	0.024	0.058	0.026
L=2	512	0.10	0.038	0.077	0.032	0.077	0.031	0.023	0.013	0.047	0.023
L=3	2048	0.046	0.012	0.042	0.011	0.042	0.011	0.015	0.0058	0.025	0.0095

Table 4.1: L^2-errors for different methods, polynomial degrees and refinement levels.

Level	Elements	CG		SUPG		GLS		HDG		Mixed	
		k=1	k=2	k=1	k=2	k=1	k=2	k=1	k=2	k=0	k=1
L=0	32	$< 1\mu$	$< 1\mu$	$< 1\mu$	$< 1\mu$	$< 1\mu$	$< 1\mu$	$< 1\mu$	$< 1\mu$	$< 1\mu$	$< 1\mu$
L=1	128	$< 1\mu$	$< 1\mu$	$< 1\mu$	$< 1\mu$	$< 1\mu$	$< 1\mu$	$< 1\mu$	$< 1\mu$	$< 1\mu$	$< 1\mu$
L=2	512	0.008	0.015	0.025	0.027	0.036	0.041	0.036	0.054	0.041	0.060
L=3	2048	0.015	0.025	0.045	0.069	0.085	0.157	0.115	0.190	0.130	0.225

Table 4.2: Runtime in seconds for different methods, polynomial degrees and refinement levels ($< 1\mu$: computation time below one microsecond).

Comparing the L^2-errors in Table 4.1 we see that each of the stabilized methods outperforms the Standard Galerkin approach, which is the fastest method as shown in Table 4.2. The HDG and mixed method show the best results regarding accuracy, but they are also the most expensive methods. The SUPG and GLS method coincide for order $k = 1$ as the Laplacian vanishes for polynomials of degree 1. Since the results for the SUPG and GLS method are very similar for order $k = 2$ we only consider the SUPG method as comparison to the HDG and mixed method in the following sections due to the lower computational cost. Most of the terms in the residuum vanish for our testcase since we use constant coefficients, whereas the coefficients in the EHL problems are non-linear functions of the pressure. Thus, the additional terms result in higher computational complexity for the SUPG method, while the complexity of the HDG and mixed method remains similar, which can be seen in section 4.3.1.

4.2 Line contact problem

We consider the same line contact problem as described in [1] for a single-body and two-body simulation. The mass-conserving cavitation approach is investigated for the single-body problem. For both simulations we refine the mesh in the expected contact region to a mesh size of 0.01 mm.

4.2.1 Single-body problem

The solutions of the EHL simulations are compared for the CG, SUPG, HDG and HM3F formulation. As density model we use the Dowson-Higginson model (2.15) and for the viscosity the Modified WLF model (2.17). The distance between the bodies is calculated analytically using equation (2.19) and the elasticity problem is solved with the equivalent material parameters for the Young's modulus and the Poisson's ratio (2.20). The meshed planar body is depicted in Figure 4.2. As initial

guess for the Newton solver we calculate the solution of the EHL equations without the load balance equation and a fixed $h_0 = 0.5$ µm instead. For each of the four formulations solutions for a maximum pressure of $p_{\max}/\text{GPa} = 0.5, 1.0, 1.5, 2.0, 2.5, 3$ are computed. This is done by increasing the force F in the load balance equation and the solution of the previous step serves as initial guess for the Newton solver. Another strategy to obtain these solutions is decreasing the rigid body displacement h_0 of the film thickness equation (2.19). For the second approach we do not consider the load balance equation and only solve the Reynolds and elasticity equation as for the initial guess of h_0. However, this leads to less control if we want to reach a certain maximum pressure as the load is not known beforehand.

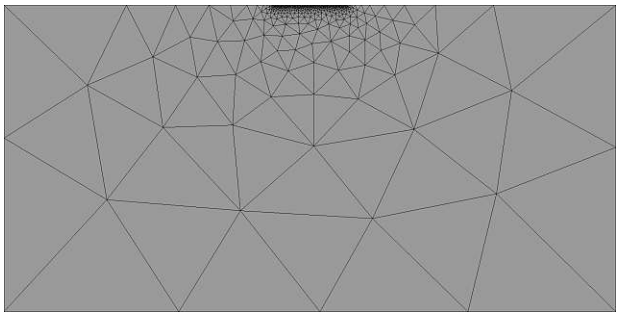

Figure 4.2: Mesh of the planar body for the line contact problem.

The parameters of the simulation are summarized in Table 4.3, which also contains the equivalent material parameters for the single-body simulation.

Parameter	Value	Parameter	Value
R (mm)	15	ρ_r (kg/m^3)	846
Velocity U (m/s)	1	μ_g (Pa.s)	10^{12}
Volume elements	1050	A_1 (°C)	19.17
Boundary elements	198	A_2 (MPa^{-1})	$4.07 \cdot 10^{-3}$
Elasticity space order k_u	2	B_1	0.23
Pressure space order k_p	3	B_2 (MPa^{-1})	0.0249
Elastic DOFs	4598	C_1	16.04
Hydrodynamic DOFs [CG, SUPG]	565	C_2 (°C)	18.18
Hydrodynamic DOFs [HDG]	960	$T_g(0)$ (°C)	-73.86
Hydrodynamic DOFs [HM3F]	2484	T (°C)	40
Equiv. Young's modulus E (GPa)	100		
Equiv. Poisson's ratio ν	0.3		

Table 4.3: Simulation Parameters: Single-body line contact problem

The degrees of freedom (DOFs) represent the total number of independent vari-

ables resulting from the discretization, corresponding to the size of the nonlinear system solved by the Newton method. In Figure 4.3a the pressure solutions of the CG formulation are depicted for different maximum pressures. The solutions show oscillations for high loaded contacts which is the reason for the introduction of stabilized methods. All of the stabilized methods lead to smooth pressure solutions, which can be seen in Figures 4.3b, 4.3c and 4.3d. Therefore, we will consider a circular contact problem in section 4.3 for a more detailed comparison of the stabilized methods with regard to quality of the solution and computational costs. An advantage of the HDG and HM3F formulation compared to the SUPG formulation is, that both methods allow two-body simulations without major modifications. This is not the case for the SUPG method as ∇h has to be computed for the residuum and h includes the calculated mesh distance of the contacting bodies.

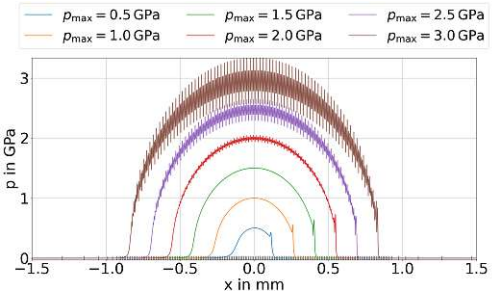

(a) CG solutions

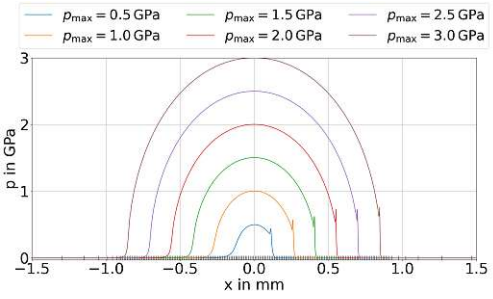

(b) SUPG solutions

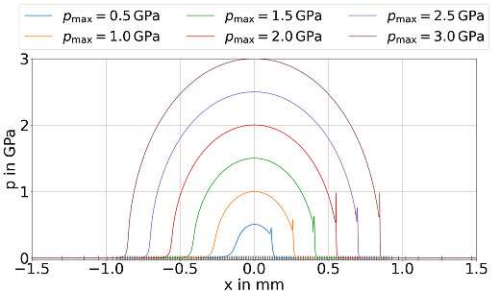

(c) HDG solutions

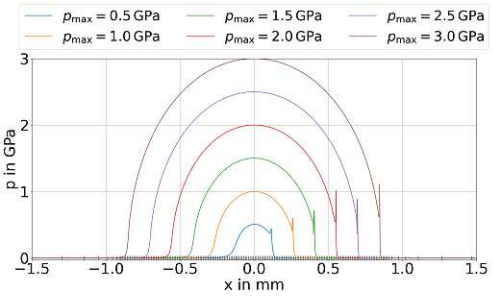

(d) HM3F solutions

Figure 4.3: Single-body line contact problem: Solution comparison for different formulations

Cavitation treatment

We use the mass-conserving cavitation model with the damping function f from equation (2.18) for the line contact problem with the same parameters as in section 4.2.1 and the HDG formulation for the Reynolds equation. The parameter η is initially set to 10^8 Pa and decreased to 10^6 Pa for the initial solution with

$h_0 = 0.5$ µm. For the subsequent solutions with increased load the parameter η is kept constant until a maximum pressure of $p_{\max} = 2.5$ GPa is reached. After reaching the maximum pressure $p_{\max}$, η is further decreased to 10^4 Pa to reduce the negativity of the final pressure solution. The minimum pressure values for each η value are summarized in Table 4.4 and the corresponding pressure solutions in the outlet region are depicted in Figure 4.4.

η (Pa)	$4.0 \cdot 10^5$	$1.6 \cdot 10^5$	$6.5 \cdot 10^4$	$2.6 \cdot 10^4$	$1.0 \cdot 10^4$
Minimum Pressure (MPa)	-0.8076	-0.3845	-0.1788	-0.0817	-0.0368

Table 4.4: Minimum pressure values for different η values.

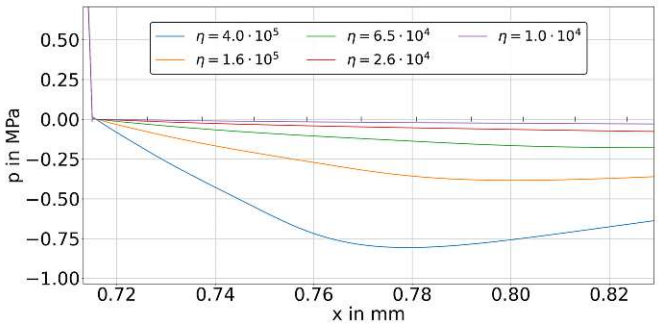

Figure 4.4: Comparison of the pressure solution in the outlet region for different η values.

4.2.2 Two-body problem

Considering the same line contact problem as in section 4.2.1 we now simulate both bodies and calculate the film thickness via the distance of the two surfaces instead of an analytic expression.

Parameter	Value	Parameter	Value
Volume elements	2722	Elastic DOFs	11696
Boundary elements	402	Hydrodynamic DOFs [CG]	565
Elasticity space order k_u	2	Hydrodynamic DOFs [HDG]	1362
Pressure space order k_p	3	Poisson's ratio $\nu_1 = \nu_2$	0.3
		Young's modulus $E_1 = E_2$ (GPa)	200

Table 4.5: Simulation Parameters: Two-body line contact problem

The parameters for density and viscosity are the same as in Table 4.3 and the remaining updated parameters are summarized in Table 4.5. The meshed geometry is depicted in Figure 4.5, where the mesh of the planar body coincides with the mesh used in the single-body problem from Figure 4.2. Similar to the

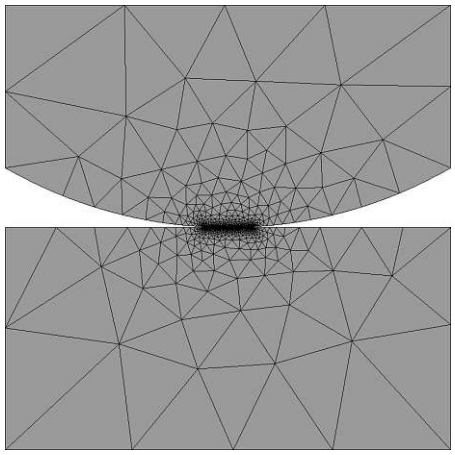

Figure 4.5: Mesh of both bodies for the line contact problem.

single-body problem we compute solutions for a maximum pressure of $p_{\max}/\text{GPa} = 0.5, 1.0, 1.5, 2.0, 2.5, 3$. In Figure 4.6 the pressure solutions obtained with the CG and HDG formulation are depicted. Again the CG solutions show oscillations for high loaded contacts, whereas the HDG solutions damp these oscillations. In contrast to the single-body problem we do not obtain perfectly smooth solutions with the HDG formulation. These minor oscillations arise due to the numerical evaluation of the distance between the two bodies via the meshes. The distance

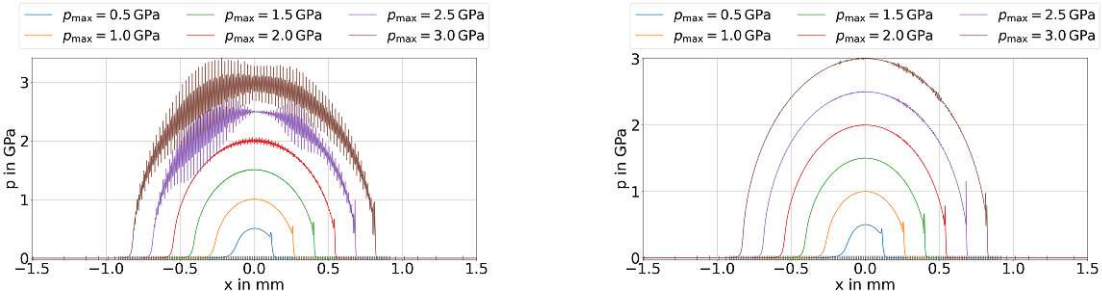

(a) CG solutions **(b)** HDG solutions

Figure 4.6: Two-body line contact problem: Solution comparison for different formulations

calculation can be achieved by defining a ContactBoundary in NGSolve which

includes a built-in gap function. This gap function determines for each integration point of one surface the closest point on the other surface and computes the distance, denoted as $\widetilde{h}(x, y)$ in eq. (2.23).

4.3 Circular contact problem

The stabilized methods led to smooth single-body pressure solutions for the line contact problem. Using the same viscosity and density models as in section 4.2, we now consider a circular contact problem and compare the CG, SUPG and HDG formulations. Instead of utilizing the loadstepping strategy, we solve the EHL problem for a given load (corresponding to $p_{\max} = 2$ GPa) with the Hertzian pressure profile

$$p_{\text{init}}(x, y) = \begin{cases} p_h \sqrt{1 - \left(\frac{x}{a}\right)^2 - \left(\frac{y}{a}\right)^2}, & \text{if } \sqrt{x^2 + y^2} \leq a, \\ 0, & \text{otherwise,} \end{cases}$$

as initial pressure guess for the Newton solver. Here

$$p_h = \frac{3F}{2\pi a^2}$$

denotes the maximum Hertzian pressure and

$$a = \sqrt[3]{\frac{3FR}{2E'}} \tag{4.2}$$

is the radius of the contact circle, where E' is calculated according to (2.26). To obtain an initial guess for the deformation we solve an elasticity problem with the Hertzian pressure profile.

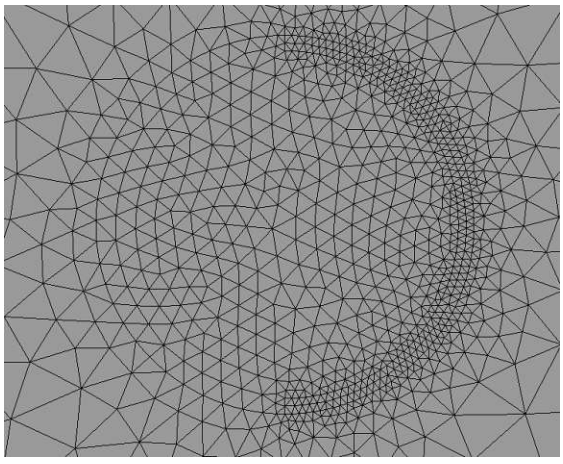

Figure 4.7: Contact boundary mesh for the circular contact problem.

The mesh is refined in the expected contact region, where we used a mesh size of 0.04 mm. The outlet region is further refined to a third of the contact mesh size. The mesh of the contact boundary is depicted in Figure 4.7. The elasticity space is globally defined with polynomial order $k_u = 2$ and for the first element layer of the contact boundary the polynomial order is increased to $k_u = 3$ as this leads to better results for the deformation and less DOFs compared to using $k_u = 3$ on the whole domain. The remaining parameters of the simulation are summarized in Table 4.6. The pressure solutions obtained with the CG, SUPG, and HDG

Parameter	**Value**
R (mm)	12.7
Velocity U (m/s)	$(1, 0)^T$
Load F (N)	552
Volume elements	15128
Boundary elements	2094
Elasticity space order k_u	2 (3 at Ω_c)
Pressure space order k_p	3
Elastic DOFs	123183
Hydrodynamic DOFs [CG, SUPG]	9144
Hydrodynamic DOFs [HDG]	32892
Poisson's ratio ν	0.3
Young's modulus E (GPa)	100

Table 4.6: Simulation Parameters: Two-body line contact problem

formulations are depicted in Figure 4.8, where the pressure distributions along the x- and y-axes are plotted for a better illustration of the oscillatory behavior. The CG formulation results in oscillatory solutions for this high loaded contact similar to the line contact problem. Calculating the circular contact problem using the SUPG and HDG formulation leads to damped oscillations. The pressure solution obtained with the SUPG formulation shows an almost smooth profile along the x-axis, whereas spurious oscillations are still present in the solution along the y-axis. Since small oscillations occur in the HDG solution as well along both axes, we add an isotropic diffusion term as described in section 3.8 to the formulations. The pressure solutions for $\rho_{\text{id}} = 0.2$, along with the x- and y-axis pressure profiles, are depicted in Figure 4.9. The SUPG solution shows a smooth profile along the x-axis but still spurious oscillations along the y-axis. A similar behavior can be observed for the HDG solution where small oscillations are still present along both axes. Choosing a larger value for ρ_{id} leads to smooth pressure solutions for all three formulations but since the isotropic diffusion term is a non-consistent term,

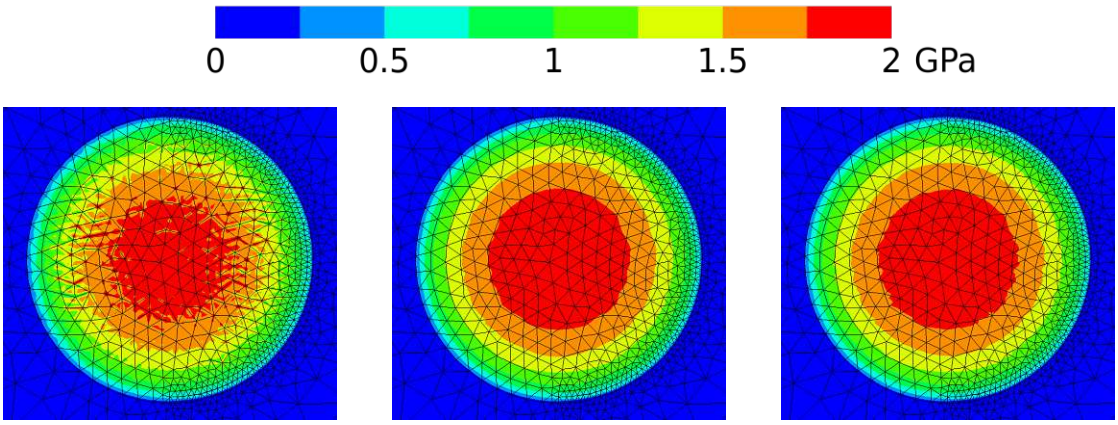

(a) CG solution (b) SUPG solution (c) HDG solution

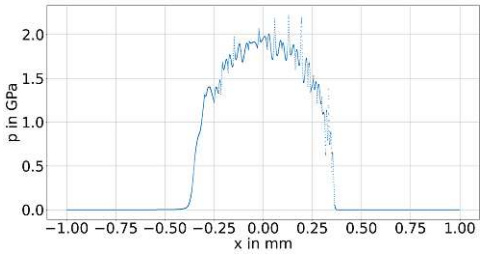

(d) CG solution along x-axis

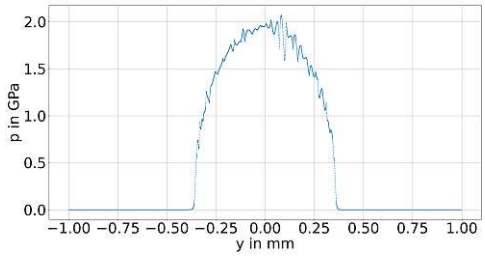

(e) CG solution along y-axis

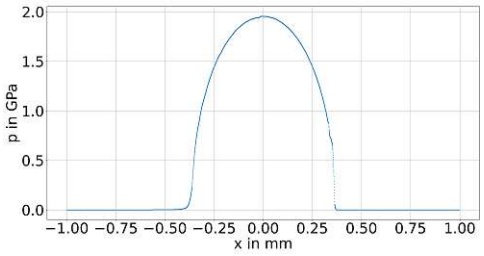

(f) SUPG solution along x-axis

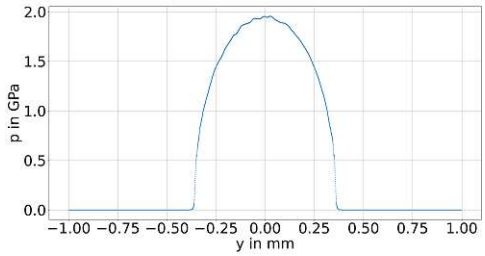

(g) SUPG solution along y-axis

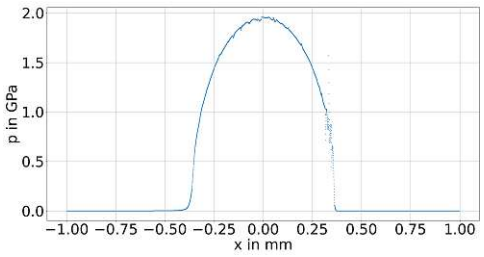

(h) HDG solution along x-axis

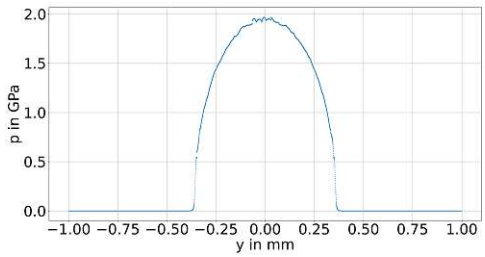

(i) HDG solution along y-axis

Figure 4.8: Single-body circular contact problem: Pressure distributions for different formulations

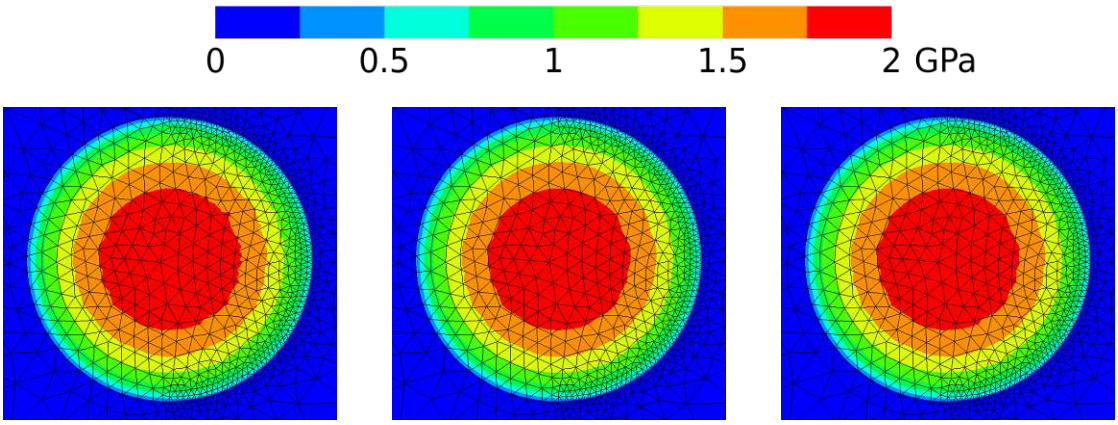

(a) CG solution (b) SUPG solution (c) HDG solution

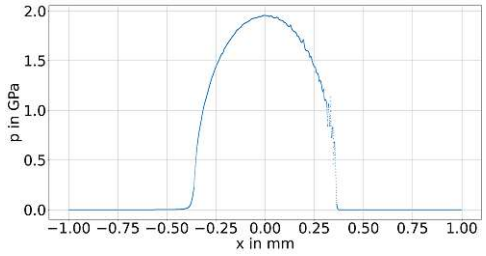

(d) CG solution along x-axis

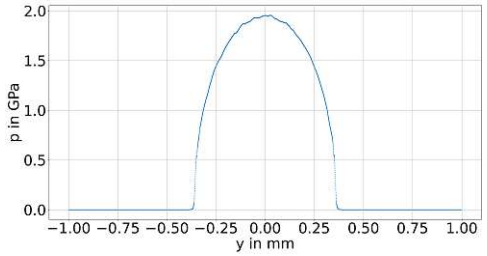

(e) CG solution along y-axis

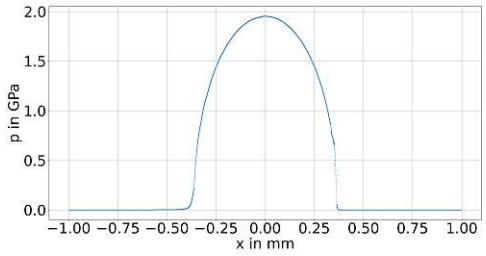

(f) SUPG solution along x-axis

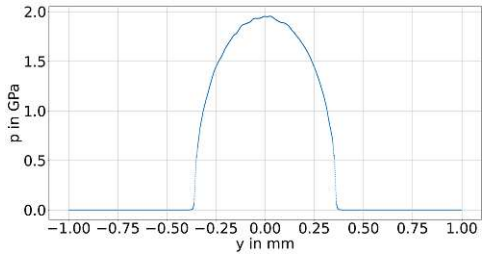

(g) SUPG solution along y-axis

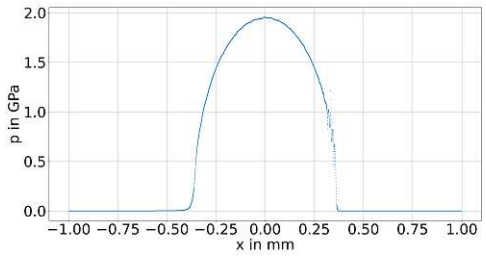

(h) HDG solution along x-axis

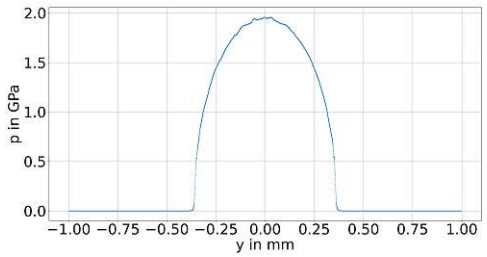

(i) HDG solution along y-axis

Figure 4.9: Single-body circular contact problem: Pressure distributions for different formulations with isotropic diffusion $\rho_{\text{id}} = 0.2$

which alters the solution, we want to keep ρ_{id} as small as possible. To demonstrate the effect of the isotropic diffusion term we consider different values for ρ_{id} and compare the minimal film thickness $h_{\min}$ and the film thickness at the center of the contact $h(0,0)$. The results are summarized in Table 4.7, where we consider the SUPG and HDG formulation for the above circular contact problem.

ρ_{id}	SUPG		HDG	
	$h_{\min}$ (nm)	$h(0,0)$ (nm)	$h_{\min}$ (nm)	$h(0,0)$ (nm)
0	30.74	114.03	31.91	114.27
0.1	29.88	113.56	30.96	113.81
0.2	29.25	113.10	30.26	113.37
0.3	28.71	112.63	29.66	112.93
0.4	28.20	112.16	29.05	112.48
0.5	27.65	111.69	28.46	112.04
0.6	27.06	111.23	27.84	111.58

Table 4.7: Comparison of minimal film thickness and film thickness at the center of the contact for different values of ρ_{id}.

4.3.1 Runtime comparison

In section 4.1 we compared the CG, SUPG and HDG formulation for a convection-diffusion problem with constant coefficients for ε and β with respect to accuracy and runtime. The HDG formulation showed the best accuracy, but was also the most expensive of the three methods. Since there is no analytical solution for the EHL problem, we cannot compare the methods with respect to accuracy. However, we can investigate the methods with regard to runtime for the circular contact problem. The results are summarized in Table 4.8, where we consider different mesh sizes for the contact region and measure the time for one Newton iteration. The number of DOFs for the CG/SUPG and HDG formulation are also listed in the table. As expected, the CG formulation exhibits the lowest computational complexity, but the results from the previous sections demonstrate that this method is prone to oscillations for high loaded contacts. Due to the expensive residual evaluation of the SUPG method for EHL problems the HDG method outperforms the SUPG method in terms of computational cost.

Mesh size (mm)	DOFs [CG / HDG]	CG (s)	SUPG (s)	HDG (s)
0.08	60510 / 70846	4.10	5.57	4.40
0.07	74172 / 86187	6.20	8.01	6.71
0.06	86904 / 101436	7.13	8.97	7.41
0.05	116772 / 135347	11.75	14.36	13.09
0.04	132327 / 156077	13.84	16.42	15.64
0.03	207480 / 243563	33.84	36.32	35.61

Table 4.8: Time in s for one Newton iteration for different methods and contact mesh sizes for the circular contact problem.

4.3.2 Model validation

To validate our implementation we compare the results of a circular contact problem with results obtained in [1]. The parameters of the simulation are summarized in Table 4.9. As density model we use the Dowson-Higginson model (2.15) and for the viscosity the isothermal Roelands model (2.16). The Moes parameters for this simulation are calculated according to equations (2.27) and result in $M = 200$ and $L = 10$.

Parameter	Value	Parameter	Value
R (mm)	16	Poisson's ratio ν	0.3
Velocity U (m/s)	$(0.8, 0)^T$	Young's modulus E (GPa)	102.83
Load F (N)	100	ρ_r (kg/m^3)	860
Elasticity space order k_u	2	μ_r (Pa.s)	0.04
Pressure space order k_p	3	α (GPa^{-1})	22

Table 4.9: Simulation Parameters: Circular contact problem (M=200, L=10)

In his work Habchi utilizes the symmetry of the problem and only simulates one half of the domain. As we consider the full domain for the EHL problem, we divide the amount of DOFs by two and compare the results. Furthermore, we have to nondimensionalize the film thickness values

$$h_{\text{nd}} = \frac{hR}{a^2},$$

where a is the radius of the contact area calculated with equation (4.2), h_{nd} is the nondimensional film thickness and h the film thickness in m. We used the same mesh as in Figure 4.7 with contact mesh sizes 0.08 mm, 0.04 mm and 0.02 mm and refined the outlet region with a factor 1/3.

Habchi model			**HDG model**			
DOFs	$h_{\mathrm{nd,min}}$	$h_{\mathrm{nd}}(0,0)$	mesh size (mm)	DOFs	$h_{\mathrm{nd,min}}$	$h_{\mathrm{nd}}(0,0)$
18313	0.0388	0.0810	0.08	15360	0.0378	0.0797
39836	0.0392	0.0818	0.04	30008	0.0384	0.0811
76249	0.0393	0.0822	0.02	80164	0.0389	0.0825

Table 4.10: Comparison between the results from [1] and HDG model for a circular contact problem with $M = 200$ and $L = 10$.

The pressure and film thickness solution obtained with the HDG formulation for a contact mesh size of 0.02 mm are depicted in Figure 4.10. The film thickness along the x- and y-axis is plotted in Figure 4.11.

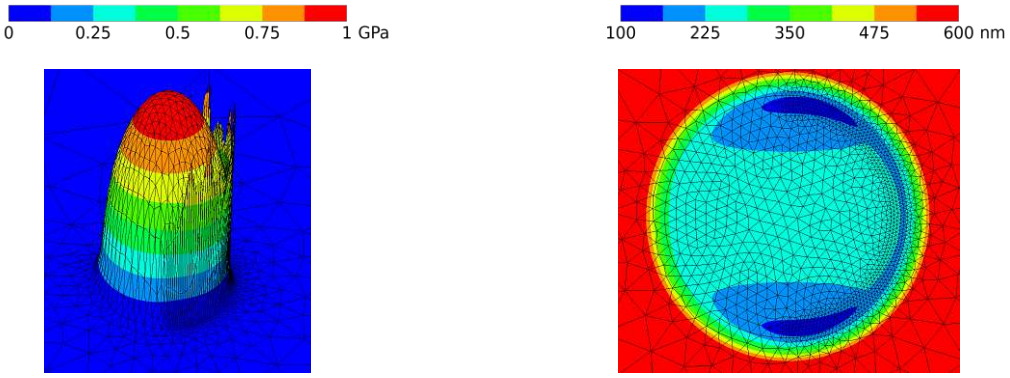

(a) Pressure solution **(b)** Film thickness solution

Figure 4.10: Pressure and film thickness solution for the circular contact problem with $M = 200$ and $L = 10$ for a contact mesh size of 0.02 mm.

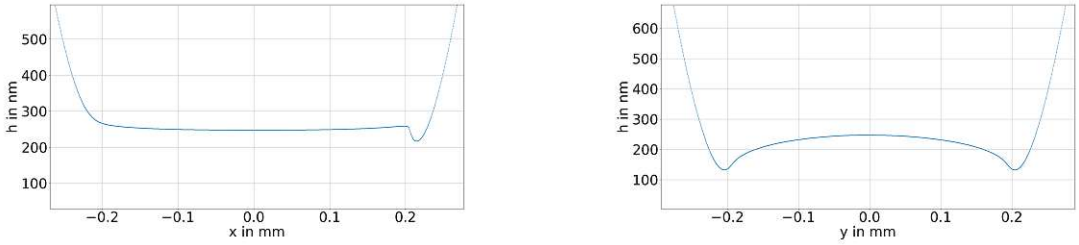

(a) Film thickness along x-axis **(b)** Film thickness along y-axis

Figure 4.11: Film thickness solution for the circular contact problem with $M = 200$ and $L = 10$.

4.4 Block on ring problem

To demonstrate the applicability of our implementation to real world problems, we consider a block on ring problem. The geometry is depicted in Figure 4.12, where the contact boundary of the ring is highlighted in red and a large gap between the bodies is chosen for better visualization.

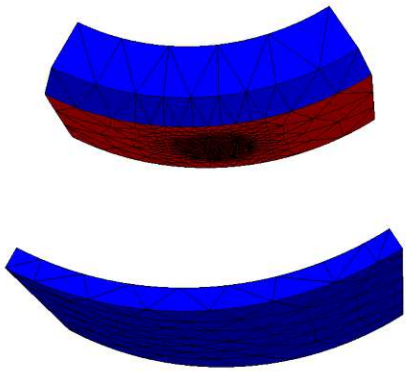

Figure 4.12: Geometry of the block on ring problem.

For the viscosity we use the isothermal Roelands model (2.16) and for the density the Dowson-Higginson model (2.15). The Reynolds equation is solved on the contact boundary of the ring. Since the mesh is not aligned with the movement direction of the ring we have to replace the vector U from equation (2.12) with the movement direction multiplied by the velocity u_m. The parameters of the simulation are summarized in Table 4.11.

Parameter	**Value**	**Parameter**	**Value**
Movement direction	$(-z, 0, x)^T$	μ_r (Pa.s)	0.0116
Velocity u_m (m/s)	5.733	α (GPa^{-1})	20
Load F (N)	8000	Poisson's ratio [ring] ν_1	0.3
Elasticity order k_u	2 / 3	Poisson's ratio [block] ν_2	0.345
Pressure order k_p	3	Young's modulus [ring] E_1 (GPa)	210
DOFs [CG]	44789 / 132737	Young's modulus [block] E_2 (GPa)	70
DOFs [HDG]	56531 / 144479	Contact domain h_{mesh} [ring] (mm)	0.4
ρ_r (kg/m^3)	846	Contact domain h_{mesh} [block] (mm)	0.4

Table 4.11: Simulation Parameters: Block on ring problem

To obtain an initial solution, we utilize the same strategy as in section 4.2, where we start with a gap $h_0 = 1$ µm and solve the EHL problem without the load

balance equation. Using the resulting pressure and deformation solution as initial guess, we solve the full EHL problem including the load balance equation and gradually increase the load until the desired load of $F = 8000$ N is reached. The pressure solutions obtained with the CG and HDG formulation are similar since we consider a moderate loaded contact with $p_{\max} = 290$ MPa. The results for the pressure and the film thickness for the simulation with elasticity order $k_u = 3$ are depicted in Figure 4.13 and Figure 4.14, respectively.

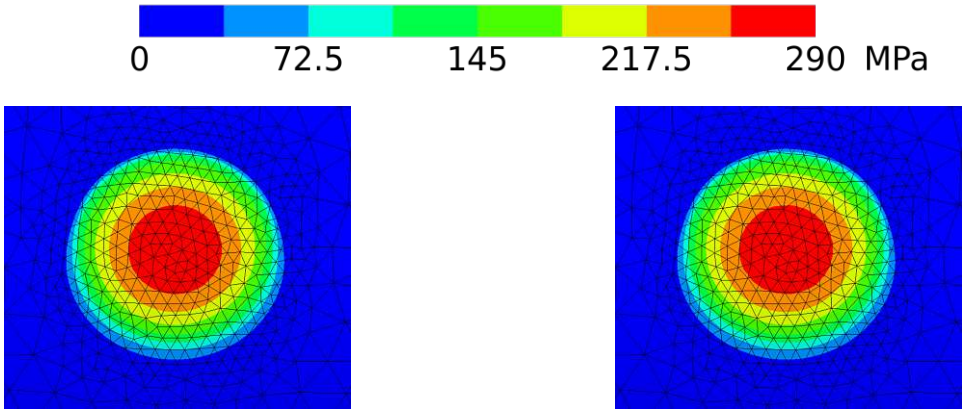

(a) CG solution **(b)** HDG solution

Figure 4.13: Block on ring problem: Comparison of pressure distributions for CG and HDG formulation with elasticity order $k_u = 3$

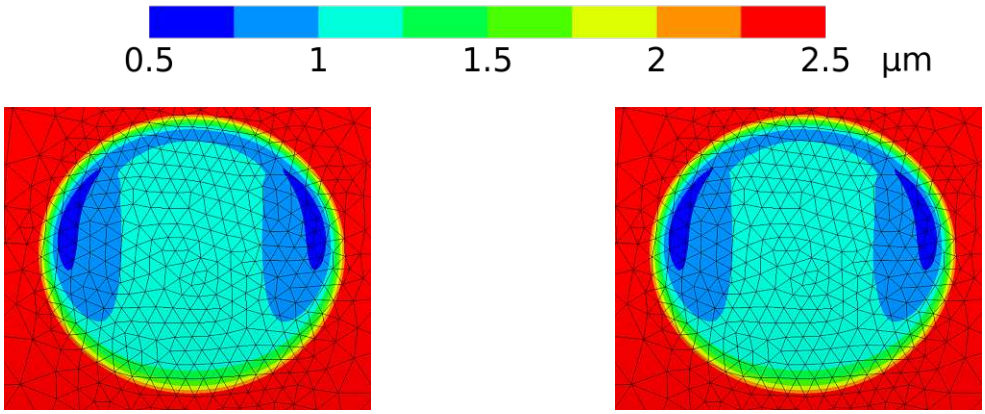

(a) CG solution **(b)** HDG solution

Figure 4.14: Block on ring problem: Comparison of film thickness solutions for CG and HDG formulation with elasticity order $k_u = 3$

To investigate the influence of the elasticity order on the solution quality, we per-

form the same simulation with elasticity order $k_u = 2$. The solutions for the pressure and the film thickness obtained with this configuration show small oscillations for both methods, which demonstrates the necessity of higher order elasticity approximations to obtain smooth solutions in EHL problems. The pressure solutions are depicted in Figure 4.15.

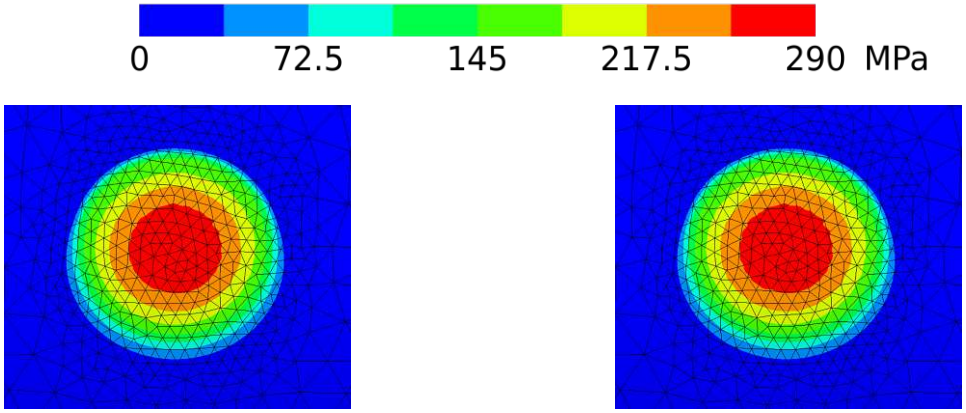

(a) CG solution **(b)** HDG solution

Figure 4.15: Block on ring problem: Comparison of pressure distributions for CG and HDG formulation with elasticity order $k_u = 2$

For a better visualization of the differences between the two simulations with elasticity orders $k_u = 2$ and $k_u = 3$, an enlarged view of the obtained pressure solutions with the CG method is shown in Figure 4.16.

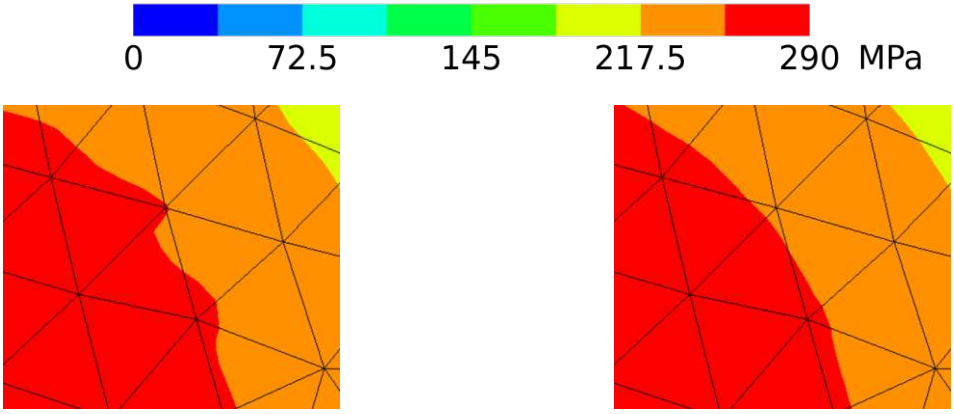

(a) CG solution with elasticity order $k_u = 2$ **(b)** CG solution with elasticity order $k_u = 3$

Figure 4.16: Block on ring problem: Comparison of pressure distributions for CG formulation with elasticity orders $k_u = 2$ and $k_u = 3$

The results for the minimal film thickness $h_{\min}$, the film thickness at the center of the contact h_c and the maximum pressure $p_{\max}$ for both formulations and elasticity orders are summarized in Table 4.12. We observe only minor differences with regard to these quantities, which indicates, that using an elasticity order of $k_u = 2$ provides sufficient result accuracy for this problem.

	HDG, $k_u = 2$	HDG, $k_u = 3$	CG, $k_u = 2$	CG, $k_u = 3$
$h_{\min}$ (µm)	0.544	0.549	0.545	0.549
h_c (µm)	1.076	1.079	1.078	1.077
$p_{\max}$ (MPa)	288.98	288.32	288.91	288.52

Table 4.12: Results for minimal film thickness $h_{\min}$ (µm), film thickness at the center of the contact h_c (µm), and maximum pressure $p_{\max}$ (MPa) for different formulations and elasticity orders.

4.4.1 Runtime comparison

Elasticity order $k_u = 3$

The complete simulation including the load stepping to reach the desired load of $F = 8000$ N took 131 min 34 s for the CG formulation. The HDG formulation was finished after 149 min 6 s which is approximately a factor 1.13. Since the load stepping strategy might lead to failed loadsteps and therefore different number of Newton iterations for both methods, we also compare the time for one Newton iteration. For the CG formulation one Newton iteration took 83.87 s on average considering the mean value of 20 iterations. The HDG formulation needed 84.80 s per Newton iteration which results in a factor of 1.01. Note that here most of the DOFs originate from the elasticity problem since we use order $k_u = 3$ for the displacement, therefore the difference in runtime is not as significant as in the previous examples. Although the HDG formulation entails greater computational complexity than the CG formulation, the results presented in the previous sections demonstrate that it produces smoother and more stable pressure solutions for high loaded contacts.

Elasticity order $k_u = 2$

The same simulation with elasticity order $k_u = 2$ took 14 min 26 s for the CG formulation and 20 min 35 s for the HDG formulation which is approximately a factor 1.42. The time for one Newton iteration was 13.08 s on average for the CG and 15.85 s for the HDG formulation, resulting in a factor of 1.21.

Since we used order $k_u = 3$ elements for the whole elasticity space for the first simulation the number of DOFs is significantly higher compared to the simulation with order $k_u = 2$. As a trade-off between solution quality and computational cost, we could apply the same strategy as in section 4.3 and only increase the polynomial order of the element layer adjacent to the contact boundary.

Chapter 5

Conclusion

In this thesis we presented stable formulations for the Reynolds equation in the context of elastohydrodynamic lubrication (EHL) problems. We discussed the implementation of a continuous Galerkin (CG), streamline upwind Petrov-Galerkin (SUPG), hybrid discontinuous Galerkin (HDG) and hybrid mixed three-field formulation (HM3F). The numerical results demonstrated the effectiveness of these methods in solving the coupled problem, with a particular focus on their performance under high loaded conditions. For problems, where the stabilized formulations still exhibited spurious oscillations, we introduced an isotropic diffusion term to further enhance solution stability and compared its influence on the solution. A runtime comparison revealed that while the HDG method is computationally more expensive than the CG method, it outperforms the latter with regard to solution quality for high loaded contacts. As a conclusion, we demonstrated the applicability of our implementation to real-world problems. Future work could focus on extending the presented formulations to thermal EHL problems, where an energy equation is solved in addition to the Reynolds and elasticity equation to account for temperature effects on the lubricant properties.

List of Figures

List of Tables

Bibliography

[1] W. Habchi. *A Full-system Finite Element Approach to Elastohydrodynamic Lubrication Problems: Application to Ultra-low-viscosity Fluids*. PhD thesis. Institut National des Sciences Appliquées (INSA), 2008.

[2] C. Lehrenfeld. *Hybrid Discontinuous Galerkin Methods for Incompressible Flow Problems*. MA thesis. RWTH Aachen, 2010.

[3] H. Egger and J. Schöberl. *A hybrid mixed discontinuous Galerkin finite-element method for convection–diffusion problems*. In: *Ima Journal of Numerical Analysis* 30 (2010), pp. 1206–1234.

[4] K. Olsson. *Cavitation in Dynamically Loaded Bearings*. Tech. rep. 308. Chalmers University of Technology, 1965.

[5] B. Jakobsson and L. Floberg. *The Finite Journal Bearing, Considering Vaporization*. Tech. rep. 190. Chalmers University of Technology, 1957.

[6] A. Almqvist and F. Pérez Ràfols. *Scientific Computing with Applications in Tribology: A course compendium*. 2022.

[7] D. Dowson and G. R. Higginson. *Elastohydrodynamic Lubrication: The Fundamentals of Roller and Gear Lubrication*. Oxford: Pergamon Press, 1966.

[8] C. Barus. *Isothermal, Isopiestics and Isometrics Relative to Viscosity*. In: *American Journal of Science* 45 (1893), pp. 87–96.

[9] H. S. Cheng and B. Sternlicht. *A Numerical Solution for the Pressure, Temperature and Film Thickness Between Two Infinitely Long, Lubricated Rolling and Sliding Cylinders, Under Heavy Loads*. In: *ASME Journal of Basic Engineering* 87 (1965), pp. 695–707.

[10] C. J. A. Roelands. *Correlational Aspects of the Viscosity-Temperature-Pressure Relationship of Lubricating Oils*. PhD thesis. The Netherlands: Technische Hogeschool Delft, 1966.

[11] J. D. Ferry. *Viscoelastic Properties of Polymers*. New York: John Wiley & Sons Inc., 1961.

[12] S. Yasutomi, S. Bair, and W. O. Winer. *An Application of a Free-Volume Model to Lubricant Rheology. Part I: Dependence of Viscosity on Temperature and Pressure*. In: *ASME Journal of Tribology* 106 (1984), pp. 291–312.

[13] D. Häggström, U. Sellgren, and S. Björklund. *Robust pre-synchronization in heavy truck transmissions*. In: *Proceedings of the International Gear Conference*. Lyon, France: Woodhead Publishing Limited, 2014, pp. 914–923.

[14] M. Soderfjall, A. Almqvist, and R. Larsson. *A model for twin land oil control rings*. In: *Tribology International* 95 (2015).

[15] M. Neunteufel. *Mixed finite element methods for nonlinear continuum mechanics and shells*. PhD thesis. Vienna: Technische Universität Wien, 2021, p. 181.

[16] B. J. Hamrock and D. Dowson. *Isothermal Elastohydrodynamic Lubrication of Point Contacts, Part III – Fully Flooded Results*. In: *ASME Journal of Lubrication Technology* 99.2 (1977), pp. 264–276.

[17] H. Moes. *Optimum similarity analysis with applications to elastohydrodynamic lubrication*. In: *Wear* 159.1 (1992), pp. 57–66.

[18] S. C. Brenner and L. R. Scott. *The Mathematical Theory of Finite Element Methods*. 2nd. Vol. 15. Texts in Applied Mathematics. New York: Springer, 2002.

[19] A. N. Brooks and T. J.R. Hughes. *Streamline upwind/Petrov-Galerkin formulations for convection dominated flows with particular emphasis on the incompressible Navier-Stokes equations*. In: *Computer Methods in Applied Mechanics and Engineering* 32.1 (1982), pp. 199–259.

[20] A.C. Galeão et al. *Finite element analysis of convection dominated reaction–diffusion problems*. In: *Applied Numerical Mathematics* 48.2 (2004), pp. 205–222.

[21] N. C. Nguyen, J. Peraire, and B. Cockburn. *An implicit high-order hybridizable discontinuous Galerkin method for nonlinear convection-diffusion equations*. In: *J. Comput. Phys.* 228.23 (Dec. 2009), pp. 8841–8855.

[22] N.C. Nguyen, J. Peraire, and B. Cockburn. *An implicit high-order hybridizable discontinuous Galerkin method for linear convection–diffusion equations*. In: *Journal of Computational Physics* 228.9 (2009), pp. 3232–3254.

[23] J. Vila-Pérez et al. *Hybridisable Discontinuous Galerkin Formulation of Compressible Flows*. In: *Archives of Computational Methods in Engineering* 28.2 (2021), pp. 753–784.

[24] P. A. Raviart and J. M. Thomas. *A mixed finite element method for second order elliptic problems*. In: *Mathematical Aspects of the Finite Element Method*. Ed. by I. Galligani and E. Magenes. Vol. 606. Lecture Notes in Mathematics. Berlin: Springer, 1977, pp. 202–315.

[25] J. Schöberl. *C++11 Implementation of Finite Elements in NGSolve*. Tech. rep. ASC Report 30/2014. Institute for Analysis and Scientific Computing, Vienna University of Technology, 2014.